Probabilistic Characterization of Nuclear-Blast Loads

Shashank Pathak, A.M.ASCE[1]; and G. V. Ramana[2]

Abstract: With increasing stockpiles of nuclear warheads, it has become essential to fortify critical infrastructure against nuclear blast. Therefore, a reliable estimation of nuclear-blast load is crucial for design of such hardened facilities. Several previous studies analyzed nonnuclear explosion scenarios without specific attention to nuclear explosions. In this paper, a standard nuclear-blast model from the literature is compared with the declassified nuclear test data, and it is observed that the standard model reasonably captures the mean trend of the decay portion of the air-overpressure history. This study accounts for the uncertainties associated with (1) the standard model, (2) occurrence of an explosion, and (3) inherent variability of nuclear-attack parameters (range, yield, and height of burst) by (1) comparing the field data with the model estimates, (2) developing a probabilistic threat scenario model, and (3) assigning appropriate probability distributions to the nuclear-attack parameters, respectively. The incorporation of these uncertainties into the standard model leads to the probabilistic characterization of nuclear-blast loads. For direct use in design, two simple equations are proposed for peak overpressure and positive phase duration in terms of probability of exceedance, and an equation is proposed that represents a normalized air-overpressure history. **DOI: 10.1061/(ASCE)ST.1943-541X.0002597.**

Author keywords: Nuclear air blast; Air overpressure; Probabilistic threat scenario; Protective structures; Uncertainties.

Introduction

With current modernization of nuclear warheads and increasing risk of terrorism, it has become essential to fortify critical infrastructure against nuclear explosions. The major effects produced by a nuclear blast are (Glasstone and Dolan 1977; Krauthammer 2008) (1) fireball, (2) radioactive and condensation cloud, (3) radiation (thermal and nuclear), (4) ejecta, fragments, and debris fall, (5) cratering, (6) moving air shock fronts, (7) ground shocks, and (8) electromagnetic pulse (EMP). All these effects produced by a nuclear detonation are critical for the design of protective structures. However, debris impact and moving air shock waves are usually of special concern to the civil engineering community.

Debris generally consists of radioactive particles, dust, dirt, weapon residue, and damaged parts of the structures during the explosion. Debris dispersion and debris throw are serious concerns because the flying debris moves along with the shock front and reaches farther locations, which may cause severe damage to structures and personnel on the way (Rempel 1981; Janser 1982; Kummer 1997; Van Der Voort and Weerheijm 2013; Rolph et al. 2014). In addition, debris may also be a limiting factor during postevent rescue operations (Edmunds et al. 1964).

Nuclear explosions release a vast amount of energy that causes a considerable increase in ambient temperature (up to a few 1,000°C) and ambient pressure (up to a few 1,000 kPa) within a very short time duration. These extreme conditions convert the surrounding air into highly compressed hot gases, which expand rapidly in form of high-pressure air shock waves (Fig. 1) and cause damage to the surrounding structures. Most of the surface structures may get destroyed at an incident air overpressure of the order of a few tens of kPa [reported in PCI-DN-14 (PCI 2004)]. Therefore, a reliable estimation of nuclear-air-blast-induced air overpressure is crucial for the design of nuclear-protective structures and is main focus of the present study.

Because nuclear-blast-resistant design is not a routine engineering problem, the classically decaying air-overpressure history caused by nonnuclear, or conventional high-explosive (HE) and chemical explosions, is mostly discussed in the current literature. The amount of energy released during a nuclear explosion may be significantly higher (a thousand to million times) compared with a conventional HE blast, due to which tremendous air overpressure is produced, which results in a comparatively longer positive phase duration (Glasstone and Dolan 1977). Unlike conventional HE explosions, in the case of nuclear explosions, an initial pressure disturbance usually arrives before the main shock wave, which is known as a precursor. In addition, the rapidly moving shock wave gets reflected when it strikes the ground surface, and these reflected waves interfere with incident wave, causing the Mach effect as shown in Fig. 1 (Glasstone and Dolan 1977). Therefore, in case of nuclear explosions, the combination of precursor and Mach effects generates various non-classically-decaying air-overpressure histories (Swift et al. 1960).

The air-overpressure histories during the positive phase duration of a typical nuclear air-blast and a typical conventional HE blast are shown in Fig. 2, and important characteristics such as rise time, peak overpressure, positive phase duration, and positive phase impulse are also explained in the figure. It can be observed from Fig. 2 that a typical conventional HE blast is associated with a shorter positive phase and lower peak overpressure compared with a typical nuclear explosion. However, in case of nuclear explosion, a significant rise time may be observed due to a precursor phenomenon. Detailed discussions on comparisons between nuclear and conventional HE blasts have been presented by Baker (1973), Command UAM (1974), Glasstone and Dolan (1977), Beshara (1994), and Krauthammer (2008).

In the literature, various models are available for defining air-overpressure history $[p(t)]$ such as (1) the linear decay model

[1]Postdoctoral Researcher, Precision Mechatronics Laboratory, Université Libre de Bruxelles, 1050 Bruxelles, Brussels, Belgium; formerly, Ph.D. Research Scholar, Dept. of Civil Engineering, Indian Institute of Technology Delhi, New Delhi 110016, India (corresponding author). ORCID: https://orcid.org/0000-0002-3868-2807. Email: shashankpathaks@gmail.com

[2]Professor, Dept. of Civil Engineering, Indian Institute of Technology Delhi, New Delhi 110016, India. Email: gvramanaiitdelhi@gmail.com

Note. This manuscript was submitted on December 26, 2018; approved on October 7, 2019; published online on February 25, 2020. Discussion period open until July 25, 2020; separate discussions must be submitted for individual papers. This paper is part of the ***Journal of Structural Engineering***, © ASCE, ISSN 0733-9445.

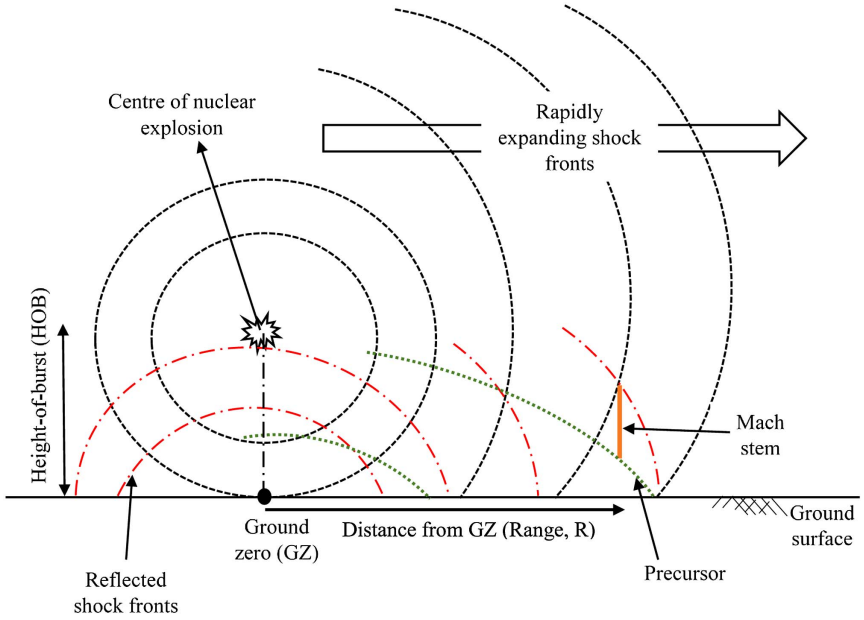

Fig. 1. Representation of nuclear-air-blast-induced precursor, reflected wavefronts, Mach stem, and moving air overpressure (shock waves) on ground surface.

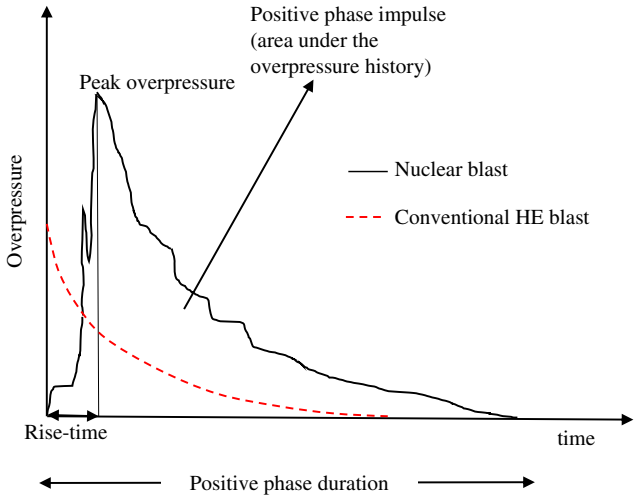

Fig. 2. Typical representation of conventional HE and nuclear-blast-induced air-overpressure histories.

(Flynn 1950), (2) two-parameter nonlinear model (Ethridge 1965), (3) three-parameter modified Friedlander model [as discussed by Baker (1973)], and (4) other nonlinear models with more than three parameters (Brode 1955, 1956, 1964). For the linear decay model, Crawford et al. (1974) provided empirical relations and charts to estimate the model parameters, but such a simple model does not capture the nonlinearity of the blast wave. On the other hand, the most popular nonlinear model (modified Friedlander's model) has been widely used for chemical (nonnuclear) explosions (e.g., Henrych 1979; Kingery and Bulmash 1984; Kinney and Grahm 1985; Bajić 2007; Teich and Gebbeken 2010).

Among these models, the empirical polynomial equations and charts developed by Kingery and Bulmash (1984) are quite popular (for example, UFC 2008; Karlos et al. 2016; Al-Rifaie and Sumelka 2017; Masi et al. 2019; Michaloudis and Gebbeken 2019) for estimation of air-blast parameters (i.e., peak overpressure, arrival time, and positive phase duration and impulse). These empirical relationships are based on a large database of several trinitrotoluene (TNT) explosions and are also used in a modern conventional weapon effects calculation tool, CONWEP (Geringer et al. 2013). Recently, the use of the CONWEP (Hyde 1991) blast-loading model [based on Kingery and Bulmash (1984) and/or TM 5-855-1 (US Army 1986)] has gained popularity due to its inclusion in the advanced numerical tools such as ABAQUS (e.g., Mougeotte et al. 2010; Lahiri and Ho 2011; Markose and Rao 2017) and Dyna2D and Dyna3D (Randers-Pehrson and Bannister 1997). A similar empirical blast model is also implemented in LS-DYNA (e.g., Neuberger et al. 2007; Gilson et al. 2012; Tabatabaei and Volz 2012). However, researchers (e.g., Le Blanc et al. 2005) also realize that even such empirical tools have significant limitations and are applicable to only nonnuclear weapons.

For nuclear explosions, the ASCE Manual 42 (ASCE 1985) provides a model for predicting air-overpressure histories as a function of height of burst (HOB), yield (W), and ground range (R) for an ideal ground surface. The model is based on the studies of Speicher and Brode (1981) and Brode (1983) and consists of a long sequence of mathematical expressions that are appropriate for calculation of peak overpressures over a range of 7 kPa to 70 MPa (ASCE 1985). Further details are available in the manual itself. The present study is carried out with three main objectives: (1) compare the ASCE (1985) model with declassified nuclear test data, (2) characterize the epistemic uncertainties associated with the model, and (3) make the model directly usable in design by combining it with an appropriate probabilistic threat scenario model that also accounts for uncertainties of the ASCE model and inherent variability of nuclear-attack parameters (R, W, and HOB).

Comparison with Experimental Records: Air-Blast Parameters

For comparison purposes, the relevant experimental data are collected from various declassified atmospheric nuclear-test reports,

and a summary of all compiled data is given in Table 1. The data belong to (1) Operation Hardtack (Swift et al. 1958), (2) Operation Plumbbob (Flathau et al. 1959; Albright et al. 1960; Bowen et al. 1960; Bultmann et al. 1960; Deeds et al. 1960; Swift et al. 1960; Perret 1960; Albright et al. 1961; Bryant and Keefer 1962), (3) Operation Redwing (Perret 1956; Kingery et al. 1960), (4) Operation Tumbler (Salmon and Hornig 1953), and (5) Operation Upshot-Knothole (Perret and Gentry 1955). In a few cases, the data were collected with multiple recording gauges at the same distance from ground zero (GZ) (Table 1). The difference between such multiple measurements shows the inherent and spatial variability of the air overpressure.

A comparison of recorded and predicted air-blast parameters, namely, shock arrival time, peak overpressures, positive phase impulse, and positive phase duration, is shown in Fig. 3. The predicted and recorded values match reasonably well. The error is calculated as follows:

$$\text{Error}(\%) = \frac{\text{Recorded data} - \text{Predicted data}}{\text{Recorded data}} \times 100 \qquad (1)$$

The respective histograms of percentage errors (excluding a few outliers) are also shown in Fig. 3, and the following are observed:

- In the case of shock arrival time, errors vary between −45% (overestimated) to +10% (underestimated), with maximum frequency in the range of −10% to +10%. On average, it is observed that ASCE model tends to predict a slightly late arrival (by 11%) of the air shock front at a given range.
- In the case of peak overpressure, the errors vary between −134% (overestimated) to +38% (underestimated), with maximum frequency in the range of −30% to +5%. On average, the ASCE model tends to predict higher (conservative) peak overpressures (by 27%).
- In the case of positive phase impulse, the errors vary between −69% (overestimated) to +33% (underestimated), with maximum frequency in the range of −10% to +10%. On average, the ASCE model tends to predict a marginally higher (conservative) positive phase impulse (by 2%).
- In the case of positive phase duration, the errors vary between −59% (overestimated) to +48% (underestimated), with maximum frequency in the range of −10% to +20%. On average, the ASCE model tends to predict a slightly shorter (by 7%) positive phase duration compared with the recorded data.

Comparison with Experimental Records: Air-Overpressure History

In this section, the recorded air-overpressure histories are compared with those predicted from the ASCE (1985) manual. For this purpose, 24 legible air-overpressure histories were digitized from various reports mentioned in section "Comparison with Experimental Records: Air-Blast Parameters." To decide an appropriate methodology for comparison, a preliminary study was carried out, as shown in Figs. 4 and 5, for Shot Cactus and Shot Koa (Operation Hardtack), respectively. The two cases indicate that the ASCE model assumes a zero rise time, i.e., a sudden rise to peak overpressure, and captures the decay portion of the history reasonably well. However, the perturbations present in the recorded histories are not captured by the ASCE model. In view of this, it was decided to compare only the decay portion of the recorded histories with the predicted histories by assuming that the shock wave arrives (predicted as well as recorded) at $t = 0$, as shown in Figs. 4(b, d, and f) and 5(b, d, and f).

During quantitative comparison of recorded and predicted peak overpressures, it is observed that, in some cases, the percentage errors may be as high as approximately −140% [Fig. 3(d)]. Therefore, it is found convenient to evaluate the error $[e(t_i)]$ at time instant t_i in terms of the ratio of recorded value $P_r(t_i)$ to predicted value $P_m(t_i)$ as follows:

$$e_i = \frac{P_r(t_i)}{P_m(t_i)} \qquad (2)$$

Here, it must be pointed out that (1) the comparison is being carried out only for the decaying portion of the recorded histories, and (2) the comparison can be carried out only for a length of the history that is the minimum of the two durations, namely (1) decay portion of recorded history, and (2) positive phase of the predicted history. To be consistent, the comparison is carried out at 100 equally spaced time instants, and the histograms of the error are obtained (Fig. 6). This comparison procedure is further applied to the remaining 18 histories, as shown in Fig. 7, and the errors from all 24 histories are combined in a single histogram as shown in Fig. 8. Based on this combined analysis, mean error is found to be 1.24, which indicates a reasonable match between the model and the field data. However, a significantly high standard deviation (1.56) compared with the mean error value is also observed, which indicates that the error varies significantly for different time instants and different nuclear tests.

Characterization of Uncertainties

For design purposes, the ASCE manual (ASCE 1985) can be used to estimate the air-overpressure history at a distance R from GZ caused by a nuclear explosion of known yield (W) at a known HOB. However, the estimated design load would be subject to three main types of uncertainties: (1) model uncertainties associated with ASCE model, (2) uncertainty of occurrence of an explosion with particular expected values of W, R, and HOB, and (3) inherent variations in expected values of W, R, and HOB.

It is worth mentioning here that (1) in a comprehensive risk analysis wherein all types of weapons (nuclear, chemical, and biological) are considered, the relative probability of nuclear attack would be usually low because these are highly controlled and possibility of a random attack is very low, and (2) the inherent variability of nuclear-attack parameters shall be limited because those are mostly well defined. However, it is quite possible that there would be very limited and fuzzy information available for design purposes. Hence, it is necessary to consider the inherent variability in nuclear-attack parameters.

Model Uncertainties

The engineering models are simple conceptualizations of various complicated real-life events and developed based on various simplifying assumptions, which are the main source of model uncertainties (e.g., Devooght 1998; Ang and Tang 2007). The model uncertainty is generally characterized (e.g., Netherton and Stewart 2010) by evaluating the statistics of the model uncertainty factor (β), defined as follows:

$$\beta = \frac{Y_e}{f(x_1, \ldots, x_n)} \qquad (3)$$

where Y_e = value of the experimental observation; $f(\cdot)$ represents the model; and $\{x_1, \ldots, x_n\} = n$ model input parameters.

Table 1. Summary of recorded blast parameters from various atmospheric nuclear tests

Operation	Shot	R (m)	W (kT)	HOB (m)	t_a (s)	P_o (kPa)	I_p (kPa-s)	t_p (s)
HardTack	Cactus	124	18	Surface	0.014	1,131	50.49	N/A
HardTack	Cactus	198	18	Surface	0.057	1,455	56.63	N/A
HardTack	Cactus	256	18	Surface	0.116	717	39.87	N/A
HardTack	Koa	610	1,300	Surface	0.1205	6,745	345.06	N/A
HardTack	Koa	958	1,300	Surface	0.359	1,648	177.32	N/A
HardTack	Koa	1,204	1,300	Surface	0.64	630	121.39	N/A
Plumbbob	Priscilla	137	37	213	N/A	N/A	N/A	N/A
Plumbbob	Priscilla	168	37	213	0.116	N/A	N/A	N/A
Plumbbob	Priscilla	198	37	213	0.131	2,358	84.12	0.149
Plumbbob	Priscilla	229	37	213	0.146	1,579	69.64	0.164
Plumbbob	Priscilla	259	37	213	0.163	1,524	N/A	0.197
Plumbbob	Priscilla	320	37	213	0.201	717	N/A	0.314
Plumbbob	Priscilla	411	37	213	0.268	407	45.64	0.357
Plumbbob	Priscilla	503	37	213	0.35	256	34.61	0.375
Plumbbob	Priscilla	610	37	213	0.475	220	40.47	0.57
Plumbbob	Priscilla	762	37	213	0.716	78	N/A	0.774
Plumbbob	Priscilla	914	37	213	1.046	75	25.23	0.789
Plumbbob	Priscilla	1,067	37	213	1.445	53	11.51	0.49
Plumbbob	Priscilla	1,372	37	213	N/A	N/A	N/A	N/A
Plumbbob	Priscilla	107	37	213	N/A	N/A	N/A	N/A
Plumbbob	Priscilla	107	37	213	N/A	7,107	N/A	N/A
Plumbbob	Priscilla	137	37	213	N/A	5,244	N/A	N/A
Plumbbob	Priscilla	137	37	213	N/A	5,175	N/A	0.175
Plumbbob	Priscilla	198	37	213	N/A	3,312	N/A	0.95
Plumbbob	Priscilla	198	37	213	N/A	2,760	N/A	0.162
Plumbbob	Priscilla	259	37	213	N/A	1,553	N/A	0.236
Plumbbob	Priscilla	259	37	213	N/A	1,421	N/A	N/A
Plumbbob	Priscilla	320	37	213	N/A	863	N/A	0.233
Plumbbob	Priscilla	320	37	213	N/A	952	N/A	0.195
Plumbbob	Priscilla	411	37	213	N/A	414	N/A	0.343
Plumbbob	Priscilla	411	37	213	N/A	428	N/A	0.28
Plumbbob	Priscilla	503	37	213	N/A	214	N/A	0.467
Plumbbob	Priscilla	610	37	213	N/A	112	N/A	N/A
Plumbbob	Priscilla	686	37	213	N/A	86	N/A	0.687
Plumbbob	Priscilla	762	37	213	N/A	63	N/A	0.852
Plumbbob	Priscilla	914	37	213	N/A	63	N/A	0.727
Plumbbob	Priscilla	1,067	37	213	N/A	68	N/A	N/A
Plumbbob	Priscilla	1,219	37	213	N/A	61	N/A	0.818
Plumbbob	Priscilla	1,372	37	213	N/A	51	N/A	N/A
Plumbbob	Priscilla	1,524	37	213	N/A	41	N/A	0.916
Plumbbob	Priscilla	1,829	37	213	N/A	N/A	N/A	N/A
Plumbbob	Priscilla	232	37	213	N/A	1,622	N/A	N/A
Plumbbob	Priscilla	232	37	213	N/A	1,553	N/A	0.178
Plumbbob	Priscilla	232	37	213	N/A	1,449	N/A	0.126
Plumbbob	Priscilla	317	37	213	N/A	773	N/A	0.307
Plumbbob	Priscilla	317	37	213	N/A	794	N/A	0.253
Plumbbob	Priscilla	317	37	213	N/A	759	N/A	0.256
Plumbbob	Priscilla	317	37	213	N/A	725	N/A	0.285
Plumbbob	Priscilla	415	37	213	N/A	414	N/A	0.404
Plumbbob	Priscilla	415	37	213	N/A	276	N/A	N/A
Plumbbob	Priscilla	262	37	213	N/A	1,207	N/A	0.26
Plumbbob	Priscilla	317	37	213	N/A	814	N/A	0.254
Plumbbob	Priscilla	415	37	213	N/A	387	N/A	N/A
Plumbbob	Priscilla	296	37	213	N/A	1,000	N/A	0.254
Plumbbob	Priscilla	317	37	213	N/A	841	N/A	0.206
Plumbbob	Priscilla	351	37	213	N/A	676	N/A	0.332
Plumbbob	Priscilla	351	37	213	N/A	690	N/A	N/A
Plumbbob	Priscilla	415	37	213	N/A	483	N/A	N/A
Plumbbob	Priscilla	415	37	213	N/A	386	N/A	0.361
Plumbbob	Priscilla	619	37	213	N/A	90	N/A	0.01
Plumbbob	Priscilla	695	37	213	N/A	95	N/A	0.661
Plumbbob	Priscilla	832	37	213	N/A	62	N/A	0.737
Plumbbob	Priscilla	1,198	37	213	N/A	61	N/A	0.825
Plumbbob	Priscilla	1,454	37	213	N/A	43	N/A	0.92
Plumbbob	Priscilla	1,865	37	213	N/A	34	N/A	N/A
Plumbbob	Priscilla	381	37	213	N/A	462	N/A	0.422
Plumbbob	Priscilla	418	37	213	N/A	393	N/A	0.374

Table 1. (*Continued*.)

Operation	Shot	R (m)	W (kT)	HOB (m)	t_a (s)	P_o (kPa)	I_p (kPa-s)	t_p (s)
Plumbbob	Priscilla	457	37	213	N/A	276	N/A	0.51
Plumbbob	Priscilla	488	37	213	N/A	235	N/A	N/A
Plumbbob	Priscilla	524	37	213	N/A	193	N/A	0.492
Plumbbob	Priscilla	564	37	213	N/A	149	N/A	0.573
Plumbbob	Priscilla	579	37	213	N/A	107	N/A	0.629
Plumbbob	Priscilla	646	37	213	N/A	79	N/A	0.679
Plumbbob	Priscilla	698	37	213	N/A	76	N/A	0.731
Plumbbob	Priscilla	768	37	213	N/A	72	N/A	0.83
Plumbbob	Priscilla	832	37	213	N/A	59	N/A	0.808
Plumbbob	Priscilla	875	37	213	N/A	69	N/A	N/A
Plumbbob	Priscilla	991	37	213	N/A	55	N/A	0.781
Plumbbob	Priscilla	1,381	37	213	N/A	N/A	N/A	N/A
Plumbbob	Priscilla	1,622	37	213	N/A	37	N/A	N/A
Plumbbob	Priscilla	198	37	213	0.141	1,863	97.94	0.211
Plumbbob	Priscilla	259	37	213	0.194	1,290	66.9	0.245
Plumbbob	Priscilla	320	37	213	0.255	828	53.8	0.307
Plumbbob	Priscilla	411	37	213	0.38	408	44.83	0.442
Plumbbob	Franklin	122	0.14	91	N/A	172	N/A	0.09
Plumbbob	Franklin	122	0.14	91	N/A	179	N/A	N/A
Plumbbob	Franklin	213	0.14	91	N/A	81	N/A	0.1
Plumbbob	Franklin	213	0.14	91	N/A	77	N/A	0.1
Plumbbob	Franklin	244	0.14	91	N/A	53	N/A	0.09
Plumbbob	Franklin	244	0.14	91	N/A	59	N/A	0.17
Plumbbob	Franklin	274	0.14	91	N/A	50	N/A	0.08
Plumbbob	Franklin	305	0.14	91	N/A	44	N/A	0.15
Plumbbob	Franklin	366	0.14	91	N/A	33	N/A	0.15
Plumbbob	Franklin	396	0.14	91	N/A	24	N/A	0.12
Plumbbob	Franklin	549	0.14	91	N/A	17	N/A	N/A
Plumbbob	Wilson	183	10.3	152	N/A	966	N/A	0.14
Plumbbob	Wilson	183	10.3	152	N/A	966	N/A	0.17
Plumbbob	Wilson	305	10.3	152	N/A	262	N/A	0.28
Plumbbob	Wilson	305	10.3	152	N/A	290	N/A	0.31
Plumbbob	Wilson	351	10.3	152	N/A	214	N/A	N/A
Plumbbob	Wilson	381	10.3	152	N/A	166	N/A	0.3
Plumbbob	Wilson	433	10.3	152	N/A	83	N/A	0.33
Plumbbob	Wilson	461	10.3	152	N/A	73	N/A	0.5
Plumbbob	Wilson	480	10.3	152	N/A	87	N/A	0.48
Plumbbob	Wilson	503	10.3	152	N/A	62	N/A	0.44
Plumbbob	Wilson	518	10.3	152	N/A	64	N/A	0.43
Plumbbob	Wilson	549	10.3	152	N/A	62	N/A	0.49
Plumbbob	Wilson	594	10.3	152	N/A	67	N/A	0.48
Plumbbob	Wilson	640	10.3	152	N/A	70	N/A	0.48
Plumbbob	Wilson	671	10.3	152	N/A	64	N/A	0.49
Plumbbob	Wilson	732	10.3	152	N/A	54	N/A	0.53
Plumbbob	Wilson	792	10.3	152	N/A	46	N/A	0.55
Plumbbob	Wilson	914	10.3	152	N/A	43	N/A	0.61
Plumbbob	Hood	305	71	488	N/A	593	N/A	0.41
Plumbbob	Hood	305	71	488	N/A	635	N/A	0.49
Plumbbob	Hood	461	71	488	N/A	359	N/A	0.54
Plumbbob	Hood	518	71	488	N/A	328	N/A	0.71
Plumbbob	Hood	671	71	488	N/A	127	N/A	0.84
Plumbbob	Hood	732	71	488	N/A	117	N/A	0.81
Plumbbob	Hood	914	71	488	N/A	59	N/A	N/A
Plumbbob	Hood	1,219	71	488	N/A	46	N/A	N/A
Plumbbob	Hood	1,219	71	488	N/A	47	N/A	N/A
Plumbbob	Hood	1,399	71	488	N/A	47	N/A	1.15
Plumbbob	Hood	1,524	71	488	N/A	43	N/A	1.17
Plumbbob	Hood	1,676	71	488	N/A	41	N/A	1.19
Plumbbob	Hood	1,829	71	488	N/A	37	N/A	1.23
Plumbbob	Hood	1,829	71	488	N/A	38	N/A	1.27
Plumbbob	Hood	2,012	71	488	N/A	32	N/A	1.33
Plumbbob	Hood	2,134	71	488	N/A	28	N/A	N/A
Plumbbob	Hood	2,438	71	488	N/A	23	N/A	N/A
Plumbbob	Hood	2,438	71	488	N/A	23	N/A	N/A
Plumbbob	Kepler	274	10.3	152	N/A	400	N/A	0.18
Plumbbob	Kepler	320	10.3	152	N/A	255	N/A	0.22
Plumbbob	Kepler	320	10.3	152	N/A	N/A	N/A	0.24

Table 1. (*Continued*.)

Operation	Shot	R (m)	W (kT)	HOB (m)	t_a (s)	P_o (kPa)	I_p (kPa-s)	t_p (s)
Plumbbob	Kepler	366	10.3	152	N/A	262	N/A	0.26
Plumbbob	Kepler	427	10.3	152	N/A	N/A	N/A	0.35
Plumbbob	Kepler	518	10.3	152	N/A	138	N/A	0.38
Plumbbob	Kepler	594	10.3	152	N/A	101	N/A	0.44
Plumbbob	Kepler	640	10.3	152	N/A	97	N/A	N/A
Plumbbob	Kepler	671	10.3	152	N/A	79	N/A	N/A
Plumbbob	Kepler	716	10.3	152	N/A	74	N/A	N/A
Plumbbob	Kepler	762	10.3	152	N/A	70	N/A	N/A
Plumbbob	Kepler	792	10.3	152	N/A	66	N/A	N/A
Plumbbob	Kepler	853	10.3	152	N/A	60	N/A	N/A
Plumbbob	Owens	152	9.7	152	N/A	1,552	N/A	0.26
Plumbbob	Owens	183	9.7	152	N/A	793	N/A	N/A
Plumbbob	Owens	183	9.7	152	N/A	707	N/A	0.15
Plumbbob	Owens	244	9.7	152	N/A	428	N/A	0.23
Plumbbob	Owens	305	9.7	152	N/A	255	N/A	N/A
Plumbbob	Owens	305	9.7	152	N/A	245	N/A	0.28
Plumbbob	Owens	351	9.7	152	N/A	186	N/A	0.35
Plumbbob	Owens	433	9.7	152	N/A	92	N/A	0.27
Plumbbob	Owens	461	9.7	152	N/A	76	N/A	0.44
Plumbbob	Owens	480	9.7	152	N/A	80	N/A	0.42
Plumbbob	Owens	503	9.7	152	N/A	59	N/A	0.46
Plumbbob	Owens	518	9.7	152	N/A	60	N/A	0.46
Plumbbob	Owens	549	9.7	152	N/A	63	N/A	0.45
Plumbbob	Owens	549	9.7	152	N/A	65	N/A	N/A
Plumbbob	Owens	914	9.7	152	N/A	41	N/A	N/A
Plumbbob	Owens	2,012	9.7	152	N/A	16	N/A	0.84
Plumbbob	Shasta	305	16.5	152	N/A	379	N/A	N/A
Plumbbob	Shasta	457	16.5	152	N/A	178	N/A	0.41
Plumbbob	Shasta	610	16.5	152	N/A	97	N/A	0.45
Plumbbob	Shasta	762	16.5	152	N/A	69	N/A	0.56
Plumbbob	Shasta	914	16.5	152	N/A	55	N/A	0.62
Plumbbob	Shasta	5,486	16.5	152	N/A	8	N/A	1.22
Plumbbob	Galileo	183	11.1	152	N/A	1,104	N/A	N/A
Plumbbob	Galileo	320	11.1	152	N/A	252	N/A	0.26
Plumbbob	Galileo	366	11.1	152	N/A	172	N/A	0.32
Plumbbob	Galileo	427	11.1	152	N/A	164	N/A	0.32
Plumbbob	Galileo	518	11.1	152	N/A	114	N/A	0.4
Plumbbob	Galileo	594	11.1	152	N/A	84	N/A	0.44
Plumbbob	Galileo	640	11.1	152	N/A	72	N/A	0.46
Plumbbob	Galileo	671	11.1	152	N/A	74	N/A	0.48
Plumbbob	Galileo	716	11.1	152	N/A	68	N/A	0.51
Plumbbob	Galileo	762	11.1	152	N/A	69	N/A	0.48
Plumbbob	Galileo	792	11.1	152	N/A	63	N/A	0.5
Plumbbob	Galileo	843	11.1	152	N/A	57	N/A	0.58
Plumbbob	Galileo	1,433	11.1	152	N/A	29	N/A	0.75
Plumbbob	Charleston	335	11.5	457	N/A	121	N/A	0.41
Plumbbob	Charleston	335	11.5	457	N/A	119	N/A	0.33
Plumbbob	Charleston	457	11.5	457	N/A	100	N/A	0.43
Plumbbob	Charleston	457	11.5	457	N/A	103	N/A	N/A
Plumbbob	Charleston	701	11.5	457	N/A	84	N/A	0.52
Plumbbob	Charleston	701	11.5	457	N/A	90	N/A	0.49
Plumbbob	Charleston	914	11.5	457	N/A	59	N/A	N/A
Plumbbob	Charleston	914	11.5	457	N/A	58	N/A	0.58
Plumbbob	Charleston	1,676	11.5	457	N/A	26	N/A	N/A
Plumbbob	Charleston	1,676	11.5	457	N/A	26	N/A	0.74
Plumbbob	Charleston	2,438	11.5	457	N/A	14	N/A	1.06
Plumbbob	Charleston	4,877	11.5	457	N/A	8	N/A	N/A
Plumbbob	Charleston	7,886	11.5	457	N/A	7	N/A	N/A
Plumbbob	Charleston	7,886	11.5	457	N/A	6	N/A	1.25
Plumbbob	Charleston	1,5611	11.5	457	N/A	2	N/A	N/A
Plumbbob	Charleston	22,250	11.5	457	N/A	1	N/A	1.58
Plumbbob	Morgan	183	8	152	N/A	655	N/A	N/A
Plumbbob	Morgan	305	8	152	N/A	228	N/A	0.28
Plumbbob	Morgan	381	8	152	N/A	138	N/A	0.4
Plumbbob	Morgan	671	8	152	N/A	53	N/A	0.46
Plumbbob	Morgan	914	8	152	N/A	39	N/A	0.57
Plumbbob	Morgan	1,524	8	152	N/A	19	N/A	0.68

Table 1. (*Continued*.)

Operation	Shot	R (m)	W (kT)	HOB (m)	t_a (s)	P_o (kPa)	I_p (kPa-s)	t_p (s)
Plumbbob	Morgan	2,012	8	152	N/A	14	N/A	0.83
Plumbbob	Morgan	2,438	8	152	N/A	10	N/A	0.84
Plumbbob	Morgan	4,572	8	152	N/A	8	N/A	N/A
Plumbbob	Morgan	6,438	8	152	N/A	6	N/A	N/A
Plumbbob	Morgan	7,886	8	152	N/A	5	N/A	0.99
Plumbbob	Morgan	7,620	8	152	N/A	2	N/A	1
RedWing	Lacrosse	210	37.8	5	N/A	2,931	N/A	N/A
RedWing	Lacrosse	280	37.8	5	N/A	1,062	N/A	N/A
RedWing	Lacrosse	344	37.8	5	N/A	931	36	0.371
RedWing	Lacrosse	427	37.8	5	N/A	379	N/A	N/A
RedWing	Lacrosse	485	37.8	5	N/A	388	N/A	N/A
RedWing	Lacrosse	594	37.8	5	N/A	248	28	0.547
RedWing	Lacrosse	762	37.8	5	N/A	123	24	0.661
RedWing	Yuma	46	0.188	61	N/A	738	N/A	N/A
RedWing	Yuma	77	0.188	61	N/A	233	2	0.038
RedWing	Yuma	111	0.188	61	N/A	166	N/A	N/A
RedWing	Yuma	122	0.188	61	N/A	145	3	0.092
Tumbler	Shot 1	51	1.05	242	N/A	185	N/A	N/A
Tumbler	Shot 1	107	1.05	242	N/A	157	N/A	N/A
Tumbler	Shot 1	179	1.05	242	N/A	100	N/A	N/A
Tumbler	Shot 1	253	1.05	242	N/A	69	N/A	N/A
Tumbler	Shot 1	328	1.05	242	N/A	75	N/A	N/A
Tumbler	Shot 1	404	1.05	242	N/A	67	N/A	N/A
Tumbler	Shot 1	480	1.05	242	N/A	54	N/A	N/A
Tumbler	Shot 1	556	1.05	242	N/A	46	N/A	N/A
Tumbler	Shot 1	632	1.05	242	N/A	36	N/A	N/A
Tumbler	Shot 1	783	1.05	242	N/A	24	N/A	N/A
Tumbler	Shot 1	935	1.05	242	N/A	17	N/A	N/A
Tumbler	Shot 2	46	1.15	338	N/A	89	N/A	N/A
Tumbler	Shot 2	192	1.15	338	N/A	68	N/A	N/A
Tumbler	Shot 2	419	1.15	338	N/A	43	N/A	N/A
Tumbler	Shot 2	648	1.15	338	N/A	32	N/A	N/A
Tumbler	Shot 2	876	1.15	338	N/A	24	N/A	N/A
Tumbler	Shot 3	51	30	1,051	N/A	77	N/A	N/A
Tumbler	Shot 3	202	30	1,051	N/A	81	N/A	N/A
Tumbler	Shot 3	429	30	1,051	N/A	70	N/A	N/A
Tumbler	Shot 3	657	30	1,051	N/A	60	N/A	N/A
Tumbler	Shot 3	885	30	1,051	N/A	52	N/A	N/A
UpshotKnothole	Shot 9	250	26	739	1.097	146	N/A	0.703
UpshotKnothole	Shot 9	390	26	739	1.237	115	N/A	0.663
UpshotKnothole	Shot 9	440	26	739	1.2988	112	N/A	0.66
UpshotKnothole	Shot 9	517	26	739	1.4	96	N/A	0.74
UpshotKnothole	Shot 9	654	26	739	1.613	77	N/A	0.767
UpshotKnothole	Shot 10	131	14.9	160	0.0915	1,655	N/A	0.188
UpshotKnothole	Shot 10	280	14.9	160	0.1915	493	N/A	0.269
UpshotKnothole	Shot 10	342	14.9	160	0.2482	253	N/A	0.313
UpshotKnothole	Shot 10	431	14.9	160	0.351	99	N/A	0.457
UpshotKnothole	Shot 10	585	14.9	160	0.596	56	N/A	0.671

Note: N/A = not available.

Model Uncertainty in Peak Overpressure and Positive Phase Duration

Because peak overpressure and positive phase duration are the two key parameters of blast load, this paper focuses on the uncertainties in the model estimates of these two parameters. To evaluate the factor β in Eq. (3), the data from Figs. 3(c and g) can be directly used in case of peak overpressure and positive phase duration, respectively, which consist of experimental observations as well as model estimates. Based on this data set, the model uncertainty factor corresponding to (1) the peak overpressure (β_{Po}), and (2) the positive phase duration (β_{tp}) are evaluated, and the corresponding histograms are obtained as shown in Fig. 9.

It is observed that both β_{Po} and β_{tp} follow a normal distribution, and the hypothesis of normal distribution is evaluated by chi-squared goodness-of-fit test. It is found that at a 5% level of significance, the chi-square test does not reject the hypothesis of a normal distribution. The parameters of normal distribution of β_{Po} are obtained as 0.84 (μ) (95% confidence interval is [0.81,0.86]) and 0.21 (σ) (95% confidence interval is [0.19,0.23]), which represent, respectively, the mean and standard deviation of the distribution. Similarly, the parameters of normal distribution of β_{tp} are obtained as 1.1027 (μ) (95% confidence interval is [1.0674, 1.1380]) and 0.2231 (σ) (95% confidence interval is [0.2015, 0.2517]).

Parametric Uncertainties

The inherent variability of blast parameters and uncertainty associated with unknown threat scenarios are important issues in the design of structures against blast loading (Stewart et al. 2006;

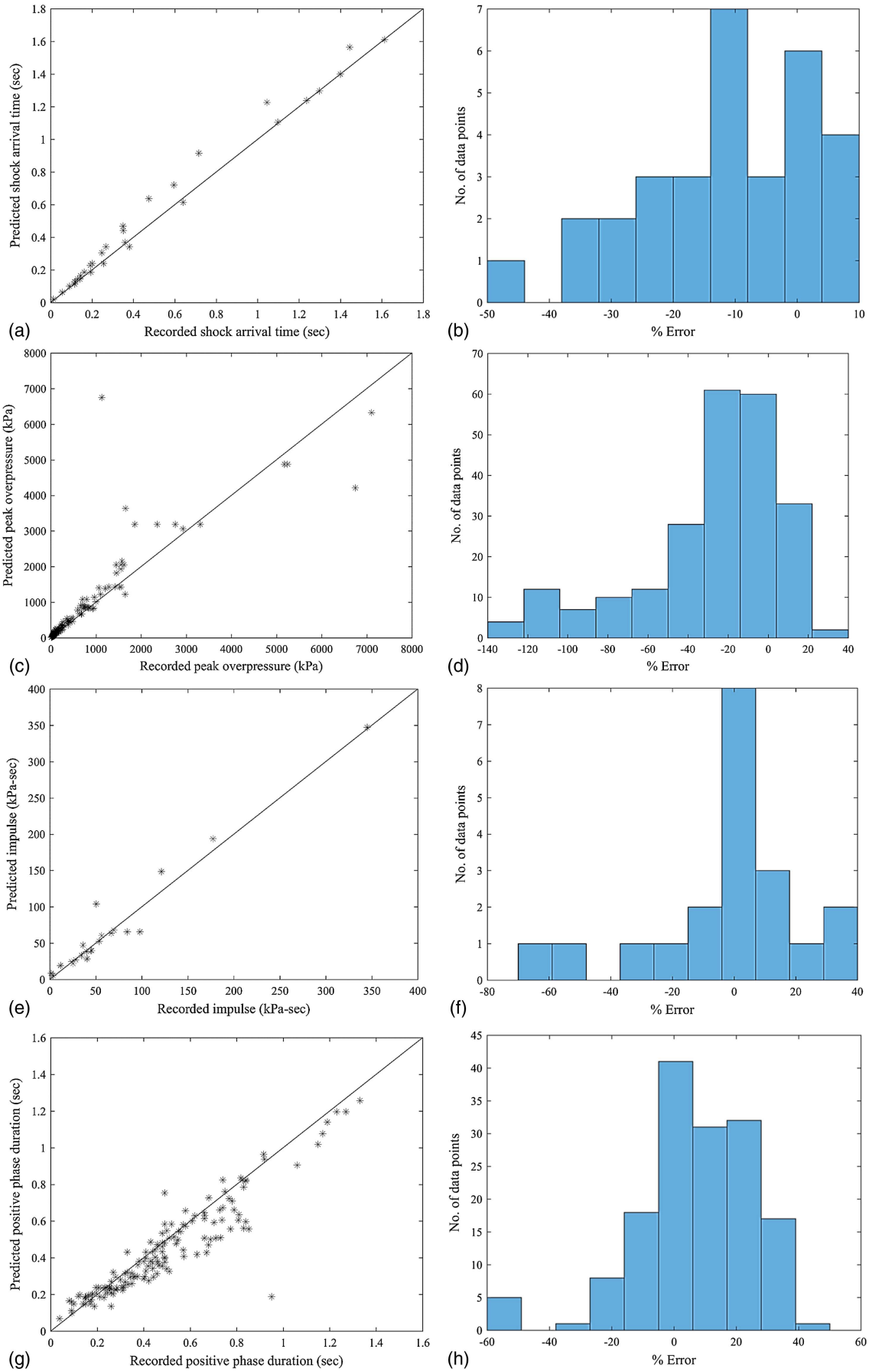

Fig. 3. Comparison between (a and b) recorded and predicted shock arrival time; (c and d) peak overpressures; (e and f) positive phase impulse; and (g and h) positive phase duration.

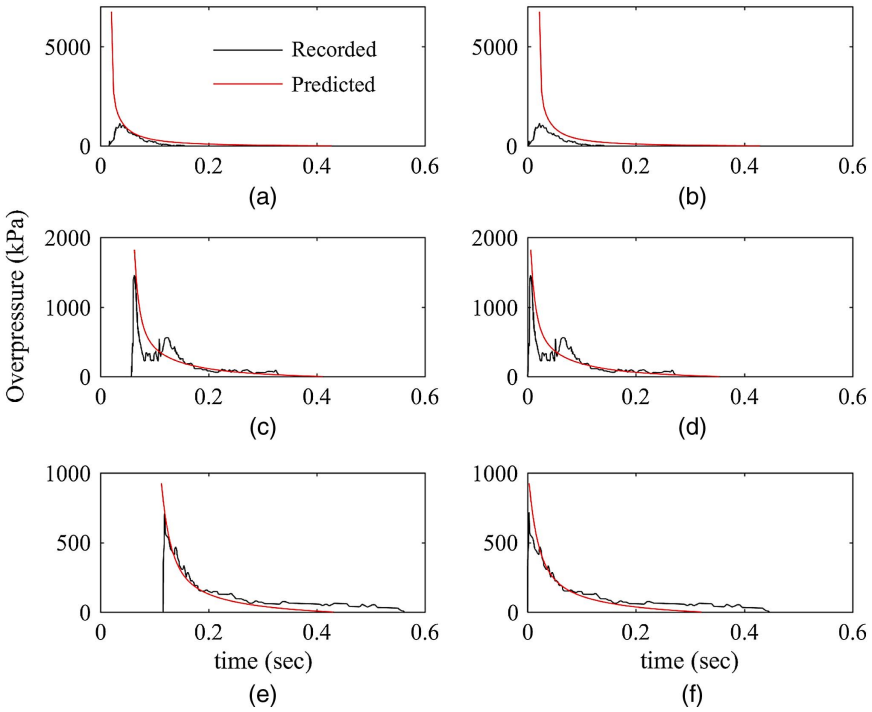

Fig. 4. Comparison of predicted air-overpressure histories from ASCE manual with recorded data at distances of (a and b) 124 m; (c and d) 198 m; and (e and f) 256 m from GZ of Shot Cactus without and with modified time axis, respectively.

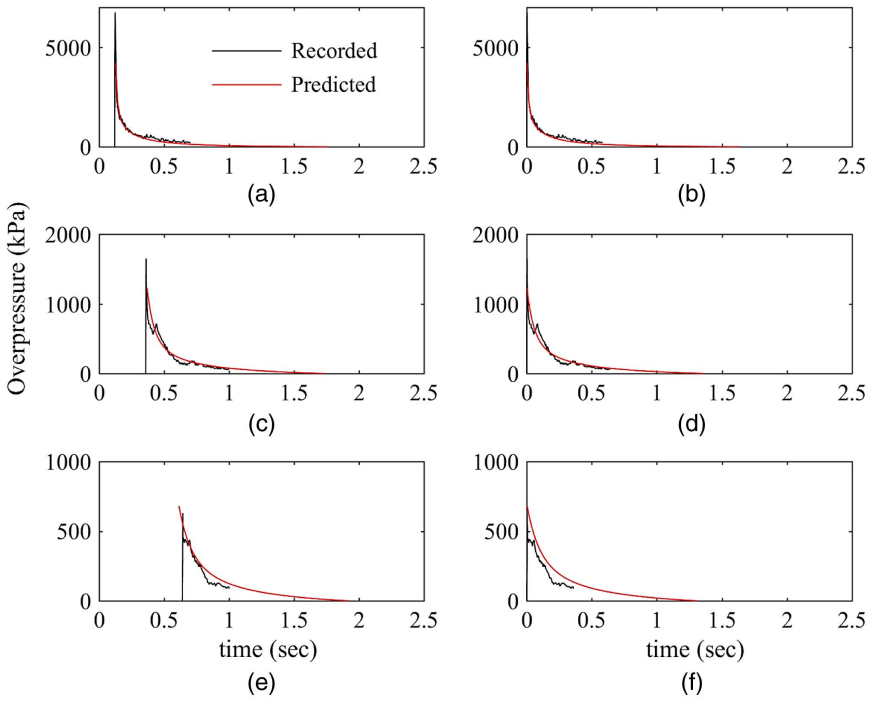

Fig. 5. Comparison of predicted air-overpressure histories from ASCE manual with recorded data at distances of (a and b) 610 m; (c and d) 958 m; and (e and f) 1,204 m from GZ of Shot Koa without and with modified time axis, respectively.

Stewart and Netherton 2008; Netherton and Stewart 2010). Because the effect of these uncertainties reflect directly on the blast-load or nuclear-attack parameters, namely distance from GZ, height of burst, and yield of explosion, these are referred here as parametric uncertainties.

For the design of nuclear-weapon-resistant facilities, usually a target analysis study is carried out that assists in the prediction of expected design air overpressures and radiation effects (Newmark and Haltiwanger 1962; Krauthammer 2008). Deciding threat scenarios along with their probabilities is an essential part of target

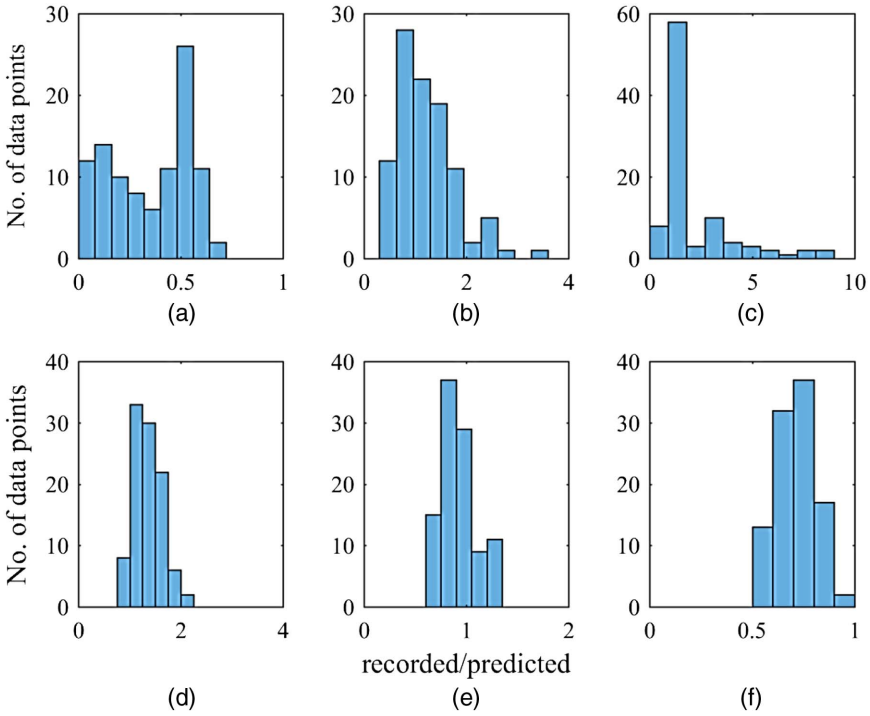

Fig. 6. Histogram of ratios of recorded overpressures to predicted overpressures at distances of (a) 124 m; (b) 198 m; and (c) 256 m from GZ of Shot Cactus; and (d) 610 m; (e) 958 m; and (f) 1,204 m from GZ of Shot Koa.

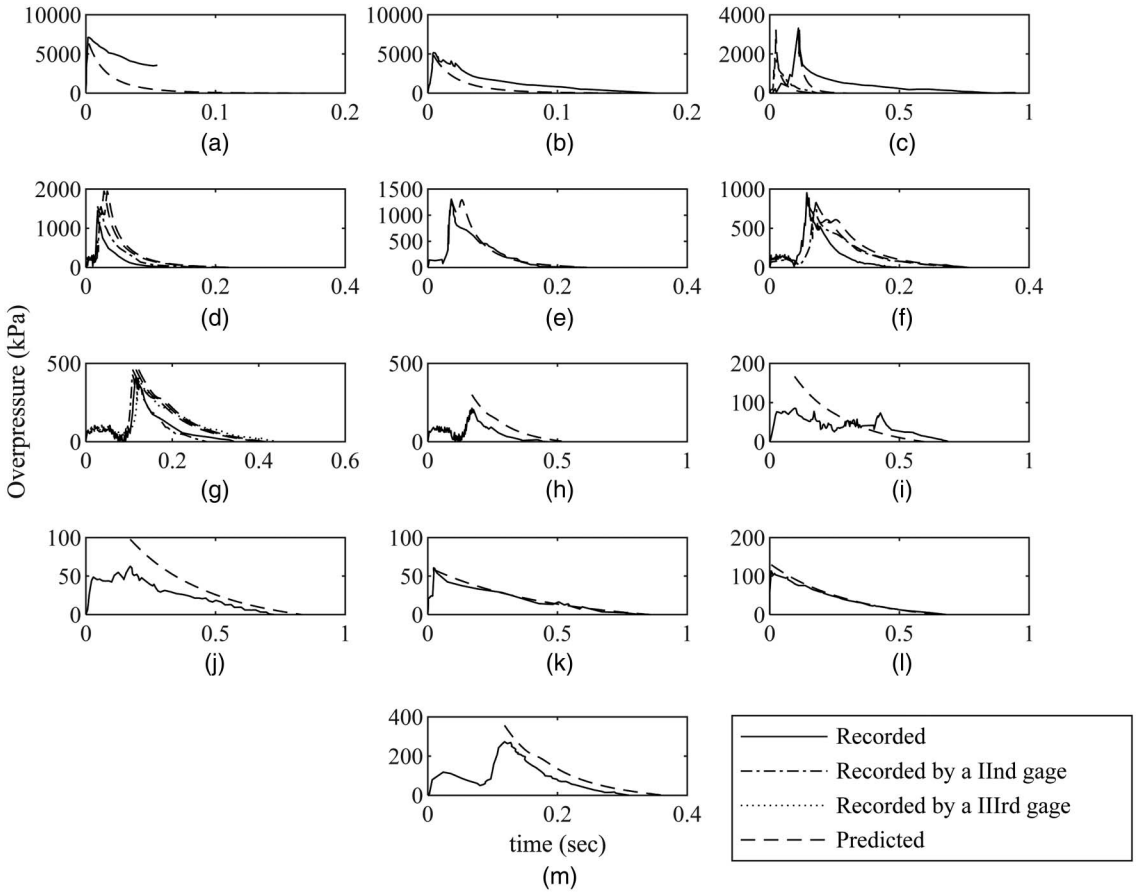

Fig. 7. Comparison of predicted and recorded air-overpressure histories at distances: (a) 107 m; (b) 137 m; (c) 198 m (from two gauges); (d) 232 m (from two gauges); (e) 259 m; (f) 320 m (from two gauges); (g) 411 m (from three gauges); (h) 503 m; (i) 686 m; (j) 914 m; (k) 1,219 m from GZ of Shot Priscilla during Operation Plumbbob; (l) 436 m from GZ of Shot 9; and (m) 341 m from GZ of Shot 10 during Operation Upshot-Knothole.

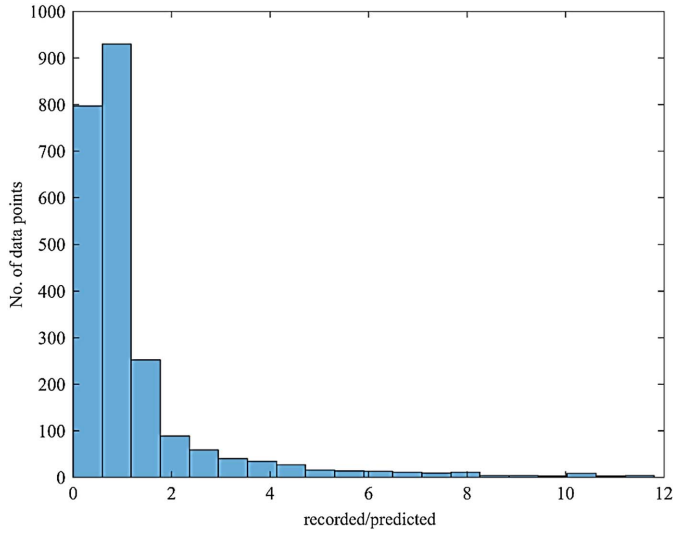

Fig. 8. Combined histogram of the ratio of recorded to predicted air-overpressure histories from all the reported events.

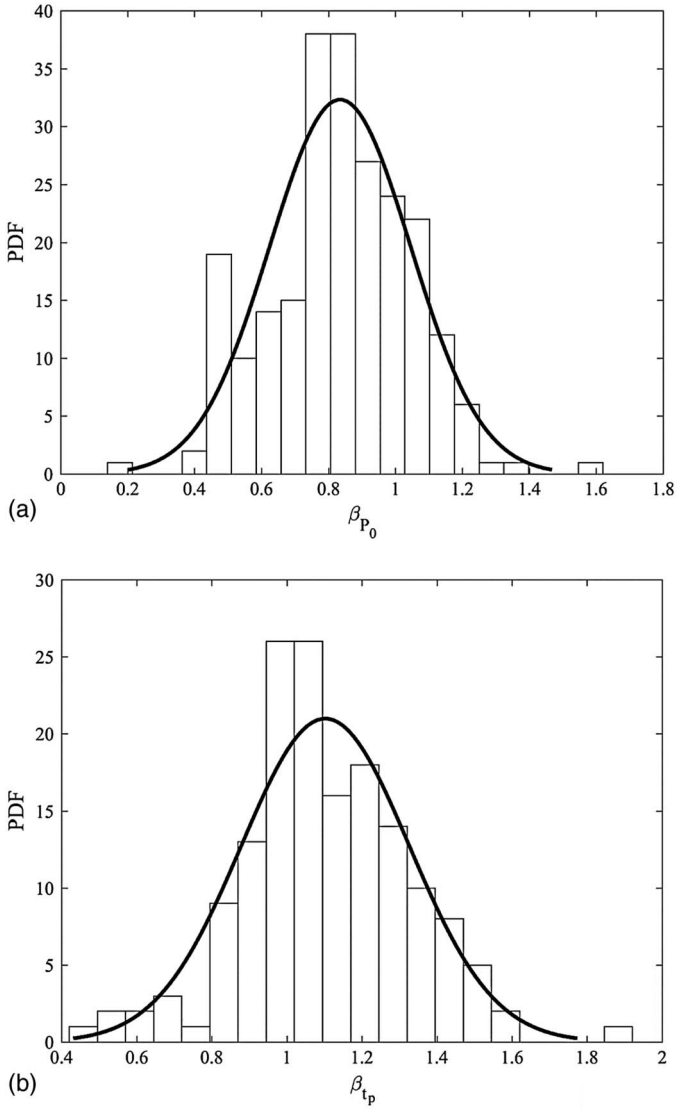

Fig. 9. Histogram and probability density function (PDF) of model uncertainty factor: (a) β_{Po}; and (b) β_{tp}.

analysis studies. In current practice, design-basis threats (DBTs) are used for the determination of the blast load for protective designs (e.g., CSA 2012; ASCE 2011). The DBTs are established by the stakeholders based on risk assessment, threat assessment, and available intelligence. The DBT is specified in terms of yield, nature (chemical or nuclear), and location of the explosion, along with the likelihood of an explosion within the targeted zone. Once DBTs are decided, the designs are developed considering the corresponding loading environments. Thus, in view of the aforementioned factors, first of all, an appropriate probabilistic threat scenario model is developed as presented in the following section.

Proposed Probabilistic Threat Scenario Model

The threat analysis is an integral part of terrorism risk analysis (e.g., FEMA 2005; Willis et al. 2006). Previously, probabilistic threat assessment of nonnuclear explosions has been discussed by Stewart and Netherton (2008), Stewart (2010), and Stewart et al. (2012). They considered explosive weights and stand-off distances as the two parameters to decide multiple threat scenarios such that a low-level threat (or highly probable threat) is considered to be associated with low yield and long stand-off, whereas, a high-level threat (or less probable threat) is taken to be associated with high yield and reduced stand-off. This paper addresses only a nuclear air-blast; therefore, the proposed threat assessment procedure includes three parameters, namely distance from GZ (R), HOB, and yield (W). If L, M, and N are the number of possible ranges, heights of burst, and yields, respectively, then there shall be a total of $L \times M \times N$ threat scenarios such that

$$\sum_{k=1}^{N}\sum_{j=1}^{M}\sum_{i=1}^{L}\Pr(\Theta_{ijk}) = 1 \tag{4}$$

where $\Pr(\Theta_{ijk})$ = relative threat probability associated with the threat scenario Θ_{ijk}, which corresponds to a range R_i, height of burst HOB_j, and yield W_k. It is assumed that the three parameters W, R, and HOB are mutually independent, and their probability mass functions (PMFs) are represented as $P_1(W)$, $P_2(R)$, and $P_3(\mathrm{HOB})$, respectively. Thus, the probabilities of occurrence of R_i, HOB_j, and W_k can be written as

$$\begin{aligned}\Pr(R_i) &= P_1(R)|_{R=R_i}\\ \Pr(\mathrm{HOB}_j) &= P_2(\mathrm{HOB})|_{\mathrm{HOB}=\mathrm{HOB}_j}\\ \Pr(W_k) &= P_3(W)|_{W=W_k}\end{aligned} \tag{5}$$

Now, the threat scenario probability can be written as

$$\Pr(\Theta_{ijk}) = \frac{\Pr(R_i)\times\Pr(\mathrm{HOB}_j)\times\Pr(W_k)}{\sum_{k=1}^{N}\sum_{j=1}^{M}\sum_{i=1}^{L}\{\Pr(R_i)\times\Pr(\mathrm{HOB}_j)\times\Pr(W_k)\}} \tag{6}$$

Let a facility of critical importance (such as a nuclear power plant, army base, nuclear shelter, or weapon storage facility) be designed to resist a nuclear air-blast. For design purposes, the nuclear air attack would be expected to occur within a certain horizontal and vertical range defined by the minimum $(R_{\min}, \mathrm{HOB}_{\min})$ and maximum $(R_{\max}, \mathrm{HOB}_{\max})$ limiting values. Thereafter, the expected attack locations (expected R and expected HOB) within the aforementioned limiting range can be decided by the security agencies or owner. In a general case, each coordinate can be associated with a probability of threat. However, to explain the developed procedure in a simplified way, it is assumed that all possible values of R and HOB are equally probable. With these assumptions, following can be written:

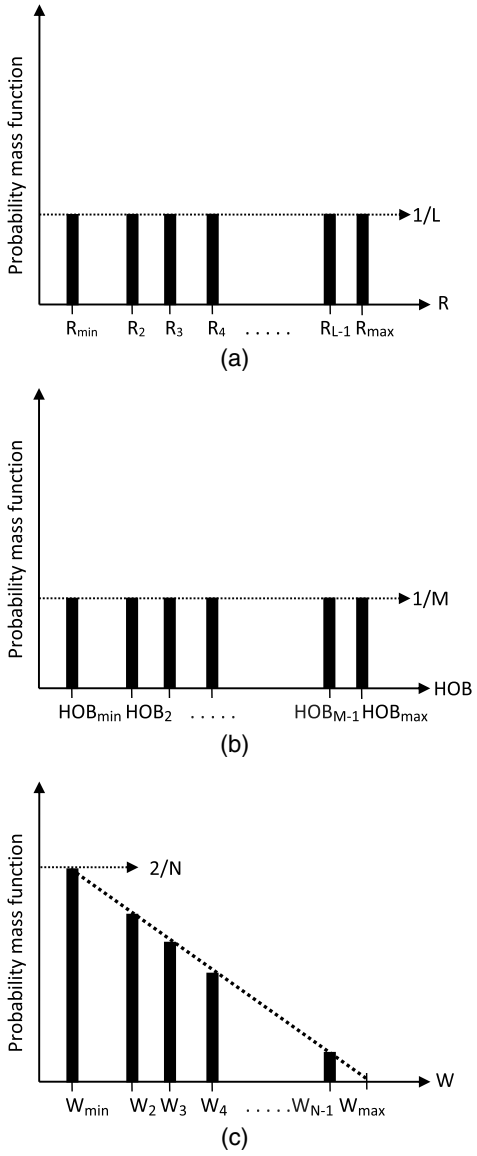

Fig. 10. Assumed probability mass functions for expected: (a) ground range (R); (b) HOB; and (c) weapon yield (W).

$$P_1(R_{\min}) = P_1(R_2) = P_1(R_3) = \ \ldots \ = P_1(R_{L-1}) = P_1(R_L) = P_1 \tag{7}$$

$$P_2(\text{HOB}_{\min}) = P_2(\text{HOB}_2) = P_2(\text{HOB}_3) = \ \ldots \ = P_2(\text{HOB}_{M-1}) = P_2(\text{HOB}_M) = P_2 \tag{8}$$

Because the total probability is equal to 1, P_1 and P_2 can be obtained as follows:

$$\sum_{i=1}^{L} P_1(R_i) = LP_1 = 1 \Rightarrow P_1 = 1/L$$

$$\sum_{j=1}^{M} P_2(\text{HOB}_j) = MP_2 = 1 \Rightarrow P_2 = 1/M \tag{9}$$

The probability mass functions of the parameters R and HOB are shown in Figs. 10(a and b). In the case of parameter W, a suitable PMF is chosen such that the probability of a nuclear threat reduces with increasing yield in a way that the highest probable yield is $W_{\min}$ and least probable (zero probability) yield is $W_{\max}$ [Fig. 10(c)]. If the probability of yield $W_{\min}$ is P_3, then the probability of other intermediate yield values are assigned in a way that probability reduces equally with each increment in yield value until $W_{\max}$. If there are N such cases, then

$$P_3(W_{\min}) = P_3; \qquad P_3(W_N = W_{\max}) = 0 \tag{10}$$

Thus, there shall be $N-1$ equal decrements of $P_3/(N-1)$ and, hence, PMFs for other intermediate yields can be written as

$$\begin{aligned} P_3(W_1) &= P_3(W_{\min}) = P_3 \\ P_3(W_2) &= P_3 - \frac{P_3}{N-1} = P_3 \times \frac{N-2}{N-1} \\ P_3(W_k) &= P_3 - \frac{P_3}{N-1}(k-1) = P_3 \times \frac{N-k}{N-1} \\ P_3(W_N) &= P_3(W_{\max}) = 0 \end{aligned} \tag{11}$$

Because the total probability is equal to 1, P_3 can be obtained as follows:

$$\sum_{k=1}^{N} P_3(W_k) = 1$$

$$\sum_{k=1}^{N} P_3 \times \frac{N-k}{N-1} = \frac{P_3}{N-1}\sum_{k=1}^{N} N-k = \frac{P_3}{N-1}\left[N^2 - \sum_{k=1}^{N} k\right] = \frac{NP_3}{2} = 1$$

$$\Rightarrow P_3 = 2/N \tag{12}$$

Using Eq. (6), the probability of various threat scenarios can be written as

$$\Pr(\Theta_{ijk}) = \frac{2(N-k)}{LMN(N-1)} \tag{13}$$

The selection of PMFs is a subjective procedure. However, the proposed procedure can be used to develop a variety of threat scenario models for different sets of probability mass functions.

Characterization of Uncertainties in Blast Parameters

A particular threat scenario (say Θ_{ijk}) provides the expected values of the three nuclear-attack parameters as R_i, HOB_j, and W_k, with a joint probability of occurrence. However, these parameters may be associated with inherent variability at the time of explosion. Recently, Campidelli et al. (2015) have shown that the uncertainties associated with the blast parameters result in significant variability in estimated overpressures. Therefore, the uncertainties associated with R_i, HOB_j, and W_k also need to be accounted for in the design procedure.

Uncertainties Associated with R_i and HOB_j. The parameters R_i and HOB_j are related to the ballistic trajectory of a weapon, which may be affected by mainly two types of errors/uncertainties (Peterson 2008): (1) ballistic dispersion error, and (2) aiming error. The ballistic dispersion error or weapon delivery error (WDE) is caused by physical inconsistencies of the weapon (weight, center of gravity, or shape), whereas the aiming error or target location error (TLE) is caused due to the difference between the actual target location and the target implemented by the weapon system, which depends upon the method of target identification [using a map or global positioning system (GPS)]. Thus, the overall uncertainty associated with explosion coordinates (R_i, HOB_j) would be a combination of WDE and TLE. The two types of errors are typically normally distributed (Driels 2004; Peterson 2008) and are usually expressed using the concept of circular error probable (CEP), which

is defined as the radius of a circle (centered on the actual target point) that has 50% probability of the weapon hitting (e.g., Pyle 1994). The CEP is more relevant in case of two-dimensional (2D) problems or surface explosions (e.g., Netherton and Stewart 2010). However, in case of air-blast, the application of the concept of spherical error probable (SEP) would be appropriate, which is a three-dimensional (3D) extension of the concept of CEP and defined as the radius of a sphere that has the 50% probability of containing the air-blast hypocenter.

If x, y, and z, are normally distributed independent coordinates of a random point in three-dimensional space, then their joint three-dimensional probability density function $f(x, y, z)$ is given as

$$f(x,y,z) = \frac{1}{(2\pi)^{3/2}\sigma_x\sigma_y\sigma_z}\exp\left[-\frac{1}{2}\left(\frac{x^2}{\sigma_x^2}+\frac{y^2}{\sigma_y^2}+\frac{z^2}{\sigma_z^2}\right)\right] \quad (14)$$

where, σ_x, σ_y, and σ_z = standard deviations of the three ordinates. Because the probability of finding the point within the sphere of radius equal to SEP is 50%, the following relation can be written:

$$\frac{1}{(2\pi)^{3/2}\sigma_x\sigma_y\sigma_z}\int_{-\mathrm{SEP}}^{\mathrm{SEP}}\int_{-\sqrt{\mathrm{SEP}^2-z^2}}^{\sqrt{\mathrm{SEP}^2-z^2}}\int_{-\sqrt{\mathrm{SEP}^2-z^2-y^2}}^{\sqrt{\mathrm{SEP}^2-z^2-y^2}}\exp\left[-\frac{1}{2}\left(\frac{x^2}{\sigma_x^2}+\frac{y^2}{\sigma_y^2}+\frac{z^2}{\sigma_z^2}\right)\right]dxdydz = 0.5 \quad (15)$$

Toma (1962) solved Eq. (15) for a case where the three standard deviations (σ_x, σ_y, and σ_z) are equal and obtained that they are equal to SEP/1.5382. For various other conditions, the solutions to Eq. (15) have been given by Schulte and Dickinson (1968). A 3D pictorial view of variability in explosion hypocenter is shown in Fig. 11 for a particular threat scenario, where a location (0, 0, 0) on the ground is to be analyzed for an explosion at location (x_t, y_t, HOB_t). For this threat scenario, the mean (or expected) value of R_i can be written as

$$R_i = \sqrt{x_t^2 + y_t^2} \quad (16)$$

However, in view of the preceding discussion, the actual location of the explosion is shifted to $(x_a, y_a, \mathrm{HOB}_a)$ with the actual range (R_a) given by

$$R_a = \sqrt{x_a^2 + y_a^2} \quad (17)$$

It is assumed that standard deviations in all three coordinates are same and equal to SEP/1.5382. If SEP is assumed to be 30 m [corresponding to the inertial navigation system (INS) guidance bomb as adopted from Netherton and Stewart (2010)], then, the standard deviation of x_a, y_a, and HOB_a would be $30/1.5382 = 19.50$ m. Now, using a Monte Carlo–simulation technique, random realizations of normally distributed variables x_a, y_a, and HOB_a are generated, and for a given random realization of x_a and y_a, the corresponding random realization of R_a is also obtained using Eq. (17). It is worth mentioning here that the random realization of R_a would always be a positive quantity, whereas a negative realization of HOB_a would correspond to an underground explosion. Because the analysis of underground explosion is beyond the scope of present work, the negative realizations of HOB_a are ignored.

Uncertainty Associated with W_k. Threat scenario modeling provides the mean or expected weapon yield, and the actual yield may vary due to the inherent variability of (1) explosive mass, and (2) the net equivalent quantity of an explosive in terms of a mass of TNT. In addition to this, the modern weapons are designed with a variable yield (dial-a-yield system) system in which the yield can be modified at any time before the attack. Therefore, such a variable-yield weapon may be subject to operational uncertainties as well. No detailed information could be located about the probabilistic distribution of the yield of nuclear weapons. However, Malik (1982) evaluated the uncertainties in estimated nuclear weapon

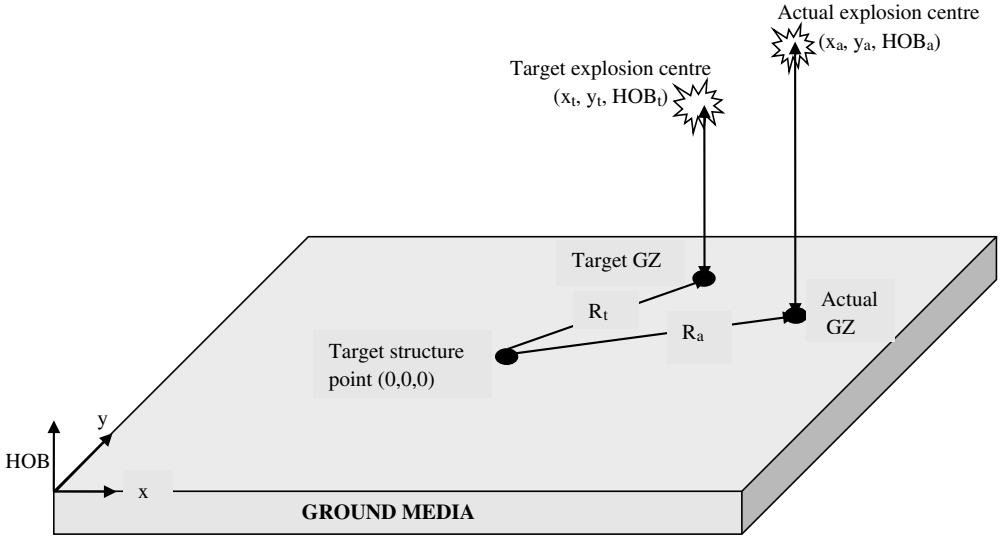

Fig. 11. Three-dimensional pictorial view of explosion hypocenter variability.

J. Struct. Eng., 2020, 146(5): 04020055

yields of the Hiroshima and Nagasaki bombing to be of the order of 20% and 10%, respectively. In view of this, the uncertainty of yield is accounted for by assuming it to be lognormally distributed (because yield cannot be negative) with a coefficient of variation of 20% (a conservative assumption for design).

Probabilistic Modeling of Nuclear-Air-Blast Load

Based on the preceding discussion, it is clear that nuclear-blast loads should be modeled probabilistically for the robust design of protective structures. To develop such a model, first of all, an exhaustive set of all the possible threat scenarios is decided by assuming parameters for the threat scenario modeling to be $R_{\min} = 100$ m, $R_{\max} = 500$ m, $\text{HOB}_{\min} = 100$ m, $\text{HOB}_{\max} = 500$ m, $W_{\min} = 10$ kT, and $W_{\max} = 500$ kT, and the considered expected values for each parameter are $R = \{100, 200, 300, 400, 500\}$ m, $\text{HOB} = \{100, 200, 300, 400, 500\}$ m, and $W = \{10, 50, 100, 200, 300, 400, 500\}$ kT. Thus, $L = 5$, $M = 5$, and $N = 7$, and hence there are a total of 175 threat scenarios for which the probabilities of occurrence are obtained using Eq. (13).

Now, the threat scenarios are selected randomly and corresponding random realizations of (1) coordinates of explosion center, and (2) yield of explosion are generated as discussed previously in this paper. Subsequently, the corresponding random realization of air-overpressure history is generated using the ASCE model. As discussed previously, the ASCE model is valid for peak overpressure within the range of 7 kPa to 70 MPa. Therefore, a random realization of air-overpressure history is valid if the corresponding peak overpressure falls with in this range.

Probability Distribution of Peak Overpressure and Positive Phase Duration

The valid realizations of air-overpressure histories also provide the valid samples of peak overpressure (P_o) and positive phase duration (t_p). However, those valid samples need to be further corrected for their respective model uncertainties (as evaluated previously in this paper). Following the previously discussed procedure and using the probability distributions of β_{Po} and β_{tp} as evaluated in Section 4.1.1., 1,000 Monte Carlo simulations are run for generating random samples of corrected peak overpressure ($\beta_{Po} \times P_o$) and corrected positive phase duration ($\beta_{tp} \times t_p$). Based on the valid samples, the resulting histograms of corrected peak overpressure and positive phase duration are obtained as shown in Fig. 12. Because β_{Po}, β_{tp}, and t_p follow a normal distribution, their negative realizations are excluded because they do not represent reality.

It is observed that corrected peak overpressure and positive phase duration follow a lognormal and normal distribution, respectively. These hypotheses are evaluated using a chi-squared goodness-of-fit test, and at 5% level of significance, the chi-square test does not reject the hypotheses. The parameters of lognormal distribution of corrected peak overpressure are obtained as 6.81 (μ) (95% confidence interval is [6.72, 6.90]) and 1.42 (σ) (95% confidence interval is [1.36, 1.47]) and those of the normal distribution of corrected positive phase duration are obtained as 0.3551 s (μ) (95% confidence interval is [0.3469, 0.3632] s) and 0.1318 s (σ) (95% confidence interval is [0.1263, 0.1379] s). The proposed probability distributions of corrected peak overpressure and positive phase duration are utilized to determine the relation of these two parameters with their corresponding probabilities of exceedance as shown in Fig. 13. Thus, the empirical equations [Eqs. (18) and (19)] are proposed for determining design peak overpressure

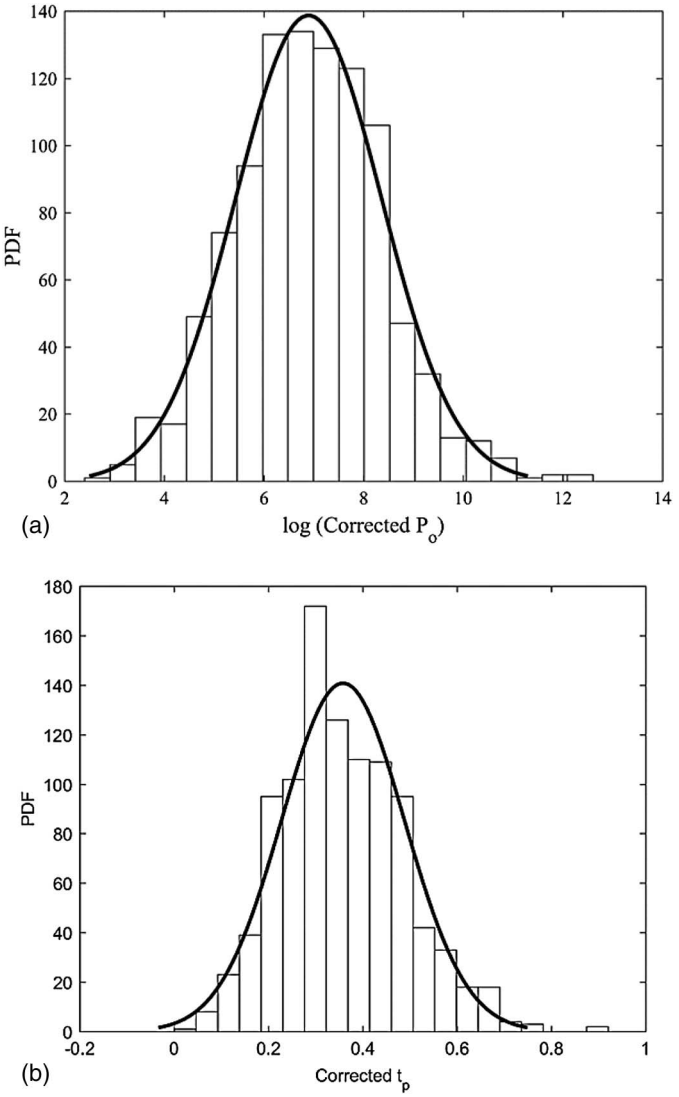

Fig. 12. Histogram and corresponding PDF of (a) logarithm of corrected peak overpressure; and (b) corrected positive phase duration.

($P_{0,\text{dgn}}$) and design positive phase duration ($t_{p,\text{dgn}}$) for a range of probability of exceedance (Pr_{ex}) from 0.05 to 0.95

$$P_{o,\text{dgn}}(\text{MPa}) = 8.41 \times \exp[-4.45 \times \text{Pr}_{\text{ex}}] \tag{18}$$

$$t_{p,\text{dgn}}(s) = 0.5614 - 0.4127 \times \text{Pr}_{\text{ex}} \tag{19}$$

Design Nuclear-Air-Blast History

Because, the statistics of peak overpressure and positive phase duration have already been analyzed, it would be sufficient to analyze the normalized air-overpressure histories such that overpressures are normalized by peak overpressure, and time instants are normalized by positive phase duration. Therefore, as discussed previously, 1,000 Monte Carlo simulations are run, and the ensemble of valid normalized histories are shown in Fig. 14(a). Each normalized history represents the shape of the overpressure waveform. To analyze the statistical distribution of these waveforms, each normalized history is tagged with the corresponding normalized positive phase impulse (area under the waveform). The histogram of normalized positive phase impulse is shown in Fig. 14(b). Because, each waveform is a discrete realization associated with a definite

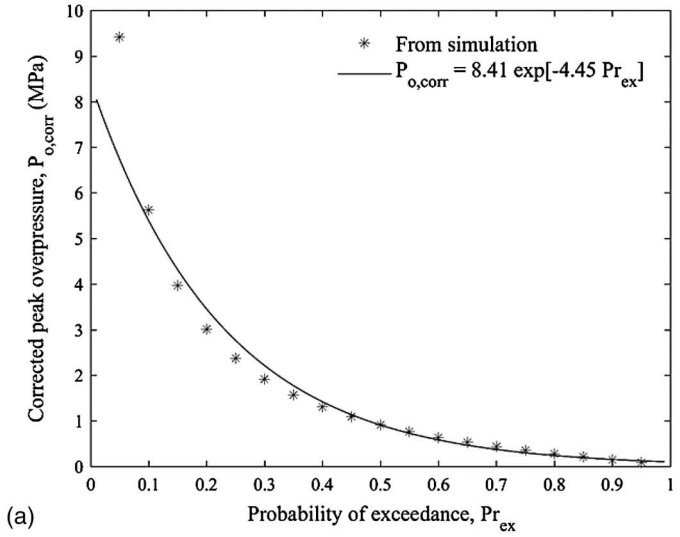

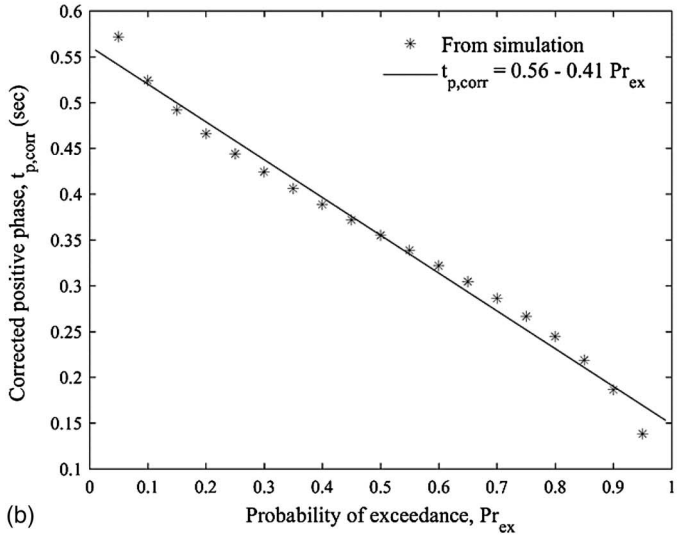

Fig. 13. Variation of the (a) corrected peak overpressure; and (b) corrected positive phase duration with their corresponding probability of exceedance.

normalized positive phase impulse, it is proposed that the waveform corresponding to the 95-percentile (or nearest to it) normalized impulse can be taken as the design waveform for the purpose of design, as shown in Fig. 14(c). The proposed design waveform fits well to the following modified Friedlander's equation

$$p_n(t_n) = (1 - t_n)e^{-bt_n} \tag{20}$$

where $p_n(t_n)$ = normalized air overpressure $(p(t)/P_o)$ at normalized time instant t_n $(= t/t_p)$; and b = decay parameter that can be estimated by regression analysis. In the present case, b is found to be 1.2978. Thus, with the help of Eqs. (18)–(20), nuclear-air-blast-induced air-overpressure history can be obtained for the purpose of design.

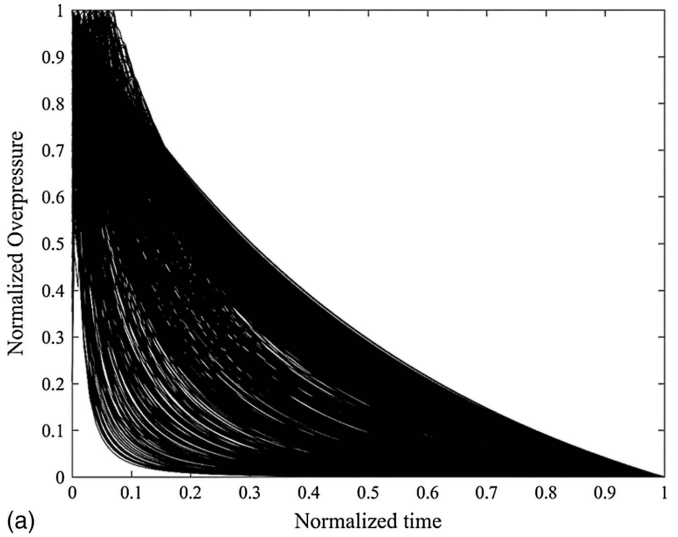

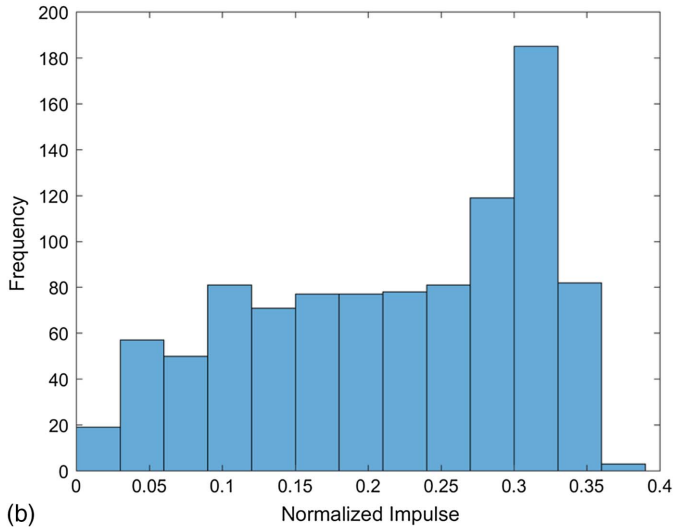

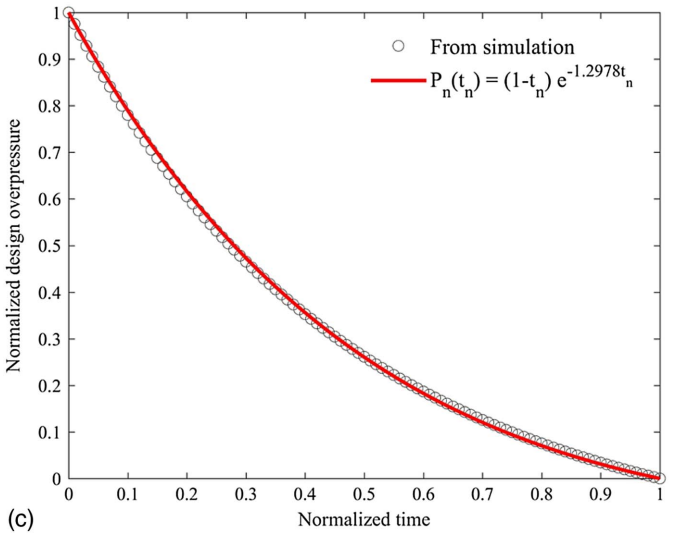

Fig. 14. (a) Ensemble of normalized air-overpressure histories; (b) histogram of normalized positive phase impulse; and (c) 95-percentile normalized air-overpressure history.

Conclusions

It has been discussed that the method given by ASCE Manual 42 is one of the most relevant models of load estimation in case of nuclear air-blasts. The ASCE model predicts air-overpressure history in terms of distance from GZ, height of burst, and yield of the explosion. Comparison of the ASCE model with field data indicated that, on average, the model predicts (1) late arrival (by 11%) of the air shock front at a given distance from GZ, (2) conservative estimates

(higher by 27%) of peak overpressures, (3) slightly shorter (by 7%) positive phase duration, and (4) positive phase impulse with excellent accuracy (average error ~ 2%). It was noticed that the ASCE model assumes a zero rise time and captures the mean trend of the decay portion of the air-overpressure history reasonably well with a mean value of the ratio of recorded to predicted air overpressure of 1.24.

However, like any other engineering model, the ASCE model also suffers from model uncertainties. In view of this, the model uncertainties were characterized, and it was found that model uncertainty factor of peak overpressure follows a normal distribution with a mean value of 0.84 and standard deviation of 0.21. Similarly, the model uncertainty factor of the positive phase duration is found to follow a normal distribution with mean value of 1.1027 and standard deviation of 0.2231. Considering the fact that the design loads must account for relevant threat scenarios, a probabilistic threat scenario model has been proposed such that a particular threat scenario represents a set of four values: (1) expected R, (2) expected HOB, (3) expected W, and (4) their joint probability of occurrence. In addition, the inherent variability caused by ballistic dispersion error, aiming error, and yield estimation errors are also accounted for in the estimation of the three parameters.

To propose a probabilistic blast model, the probabilistic threat scenario model was combined with the ASCE model, and simulated peak overpressures and positive phase durations were corrected for corresponding model uncertainties. It was found that the corrected peak overpressure and positive phase duration follow a lognormal and normal distribution, respectively. For the direct application of the probabilistic model in design, (1) empirical equations were proposed that relate the variation of peak overpressure and positive phase duration with their corresponding probabilities of exceedance, and (2) a Friedlander-type equation was proposed that represents a normalized air-overpressure history (pressures are normalized by peak overpressure and time is normalized by positive phase duration). Thus, with the help of peak overpressure, positive phase duration, and normalized air-overpressure history, the nuclear-air-blast-induced air-overpressure history can be obtained for the desired probability of exceedance.

Acknowledgments

Authors thank the anonymous reviewers for their critical assessment of the manuscript, which improved the overall quality of the paper.

References

Albright, G. H., E. J. Beck, J. C. LeDoux, and R. A. Mitchell. 1961. *Evaluation of buried corrugated-steel arch structures and associated components*. Project 3.3 (No. DASA-WT-1422). Albuquerque, NM: Defense Atomic Support Agency.

Albright, G. H., J. C. LeDoux, and R. A. Mitchell. 1960. *Evaluation of buried conduits as personnel shelters*. Project 3.2, WT-1421. Port Hueneme, CA: Naval Civil Engineering Lab.

Al-Rifaie, H., and W. Sumelka. 2017. "Numerical analysis of reaction forces in blast resistant gates." *Struct. Eng. Mech.* 63 (3): 347–359. https://doi.org/10.12989/sem.2017.63.3.347.

Ang, A. H. S., and W. H. Tang. 2007. Vol. 1 of *Probability concepts in engineering: Emphasis on applications to civil and environmental engineering*. 2nd ed. New York: Wiley.

ASCE. 1985. *Design of structures to resist nuclear weapons effects*. Manual of Practice 42. Reston, VA: ASCE.

ASCE. 2011. *Blast protection of buildings*. ASCE/SEI 59. Reston, VA: ASCE.

Bajić, Z. 2007. "Determination of TNT equivalent for various explosives." Master's thesis, Faculty of Technology and Metallurgy, Univ. of Belgrade.

Baker, W. E. 1973. *Explosions in air*. Austin, TX: University of Texas Press.

Beshara, F. B. A. 1994. "Modelling of blast loading on aboveground structures. I: General phenomenology and external blast." *Comput. Struct.* 51 (5): 585–596. https://doi.org/10.1016/0045-7949(94)90066-3.

Bowen, I., M. Franklin, and E. Fletcher. 1960. *Secondary missiles generated by nuclear-produced blast waves*. Project 33.2, WT-1468. Albuquerque, NM: Lovelace Foundation for Medical Education and Research.

Brode, H. L. 1955. "Numerical solutions of spherical blast waves." *J. Appl. Phys.* 26 (6): 766–775. https://doi.org/10.1063/1.1722085.

Brode, H. L. 1956. *Point source explosion in air*. Rep. No. RM-1824-AEC. Santa Monica, CA: Rand.

Brode, H. L. 1964. Vol. 425 of *A review of nuclear explosion phenomena pertinent to protective construction*. Santa Monica, CA: Rand.

Brode, H. L. 1983. "Analytic approximations to dynamic pressure and impulse and other fits for nuclear blasts." In *Proc., 17th Asilomar Conf. on Fire and Blast Effects of Nuclear Weapons*, 230. Washington, DC: FEMA.

Bryant, E. J., and J. H. Keefer. 1962. *Basic airblast phenomena*. Operation Plumbbob, Project 1.1, WT-1401. Albuquerque, NM: Sandia.

Bultmann, E., E. Sevin, and T. Schiffman. 1960. *Blast effects on existing upshot-knothole and teapot structures*. Project 3.4, WT-1423. Albuquerque, NM: Field Command, Defense Atomic Support Agency.

Campidelli, M., W. W. El-Dakhakhni, M. J. Tait, and W. Mekky. 2015. "Blast design-basis threat uncertainty and its effects on probabilistic risk assessment." *ASCE-ASME J. Risk Uncertainty Eng. Syst., Part A: Civ. Eng.* 1 (4): 04015012. https://doi.org/10.1061/AJRUA6.0000823.

Command UAM (Command US Army Material). 1974. *Engineering design handbook: Explosions in air part*. 1 AD/A-003 817, AMC Pamphlet AMCP 706-181. Alexandria, VA: Command Command US Army Material.

Crawford, R. E., C. J. Higgins, and E. H. Bultman. 1974. *The Air Force manual for design and analysis of hardened structures*. Rep. No. AFWL-TR-74-102. Albuquerque, NM: Air Force Weapons Laboratory.

CSA (Canadian Standards Association). 2012. *Design and assessment of buildings subjected to blast loads*. S850-12. Rexdale, ON, Canada: CSA.

Deeds, F., F. Fleming, and R. Stump. 1960. *Mine-field clearance by nuclear weapons*. Project 6.1, WT-1435. Albuquerque, NM: Field Command, DASA.

Devooght, J. 1998. "Model uncertainty and model inaccuracy." *Reliab. Eng. Syst. Saf.* 59 (2): 171–185. https://doi.org/10.1016/S0951-8320(97)00137-3.

Driels, M. R. 2004. *Weaponeering: Conventional weapon system effectiveness*, 300–302. Reston, VA: American Institute of Aeronautics and Astronautics Education Series.

Edmunds, J. E., C. K. Wiehle, and K. Kaplan. 1964. *Structural debris caused by nuclear blast*. Rep. No. URS-639-4. Burlingame, CA: United Research Services Corp.

Ethridge, N. H. 1965. *A procedure for reading and smoothing pressure-time data from H.E. and nuclear explosions*. Ballistic Research Laboratories Rep. No. 1691. Aberdeen Proving Ground, MD: Ballistic Research Laboratories.

FEMA. 2005. *Risk assessment: A how-to guide to mitigate potential terrorist attacks against buildings*. FEMA 452. Washington, DC: FEMA.

Flathau, W. J., R. A. Breckenridge, and C. K. Wiehle. 1959. *Blast loading and response of underground concrete-arch protective structures*. Project 3.1, WT-1420. Albuquerque, NM: Field Command, Defense Atomic Support Agency.

Flynn, P. D. 1950. *Elastic response of simple structures to pulse loading*. BRL Memo Rep. No. 525. Aberdeen Proving Ground, MD: Ballistics Research Laboratory.

Geringer, J. R., C. Y. Tuan, and P. D. Lindsey. 2013. "Assessment of software for blast loading and structural response analysis using a lightweight steel-joist roof as a test case." *J. Perform. Constr. Facil.* 27 (2): 144–154. https://doi.org/10.1061/(ASCE)CF.1943-5509.0000299.

Gilson, L., J. Van Roey, C. Guéders, J. Gallant, and L. Rabet. 2012. "A simple coupling of ALE domain with empirical blast load function in LS-DYNA." In Vol. 26 of *EPJ Web of Conf.*, 04018. Les Ulis, France: EDP Sciences. https://doi.org/10.1051/epjconf/20122604018.

Glasstone, S., and P. J. Dolan. 1977. *The effects of nuclear weapons*. 3rd ed. Washington, DC, US Department of Defense and Energy Research and Development Administration.
Henrych, J. 1979. *The dynamics of explosion and its use*. Amsterdam, Netherlands: Elsevier.
Hyde, D. W. 1991. *Conventional weapons program (ConWep)*. Vicksburg, MS: US Army Waterways Experimental Station.
Janser, P. W. 1982. *Lethality of unprotected persons due to debris and fragments*. Zollikon, Switzerland: Basler (Ernst) and Partners Zurich.
Karlos, V., G. Solomos, and M. Larcher. 2016. "Analysis of the blast wave decay coefficient using the Kingery–Bulmash data." *Int. J. Protective Struct.* 7 (3): 409–429. https://doi.org/10.1177/2041419616659572.
Kingery, C. N., and G. Bulmash. 1984. *Airblast parameters from TNT spherical air burst and hemispherical surface burst*. Technical Rep. No. ARBRLTR-02555. Aberdeen Proving Ground, MD: US Army Armament Research and Development Center, Ballistics Research Laboratory.
Kingery, C. N., C. H. Hoover, and J. H. Keefer. 1960. *Ground surface air-blast pressure versus distance*. Project 1.1, Operation Redwing, WT-1301. Proving Ground, MD: Army Ballistic Research Lab.
Kinney, G. F., and K. J. Grahm. 1985. *Explosive shocks in air*. Berlin: Springer.
Krauthammer, T. 2008. Vol. 22 of *Modern protective structures*. Boca Raton, FL: CRC Press.
Kummer, P. O. 1997. "Evaluation of the debris throw from the 1992 explosion in the Steingletscher installation in Switzerland." *J. Hazard. Mater.* 56 (1–2): 149–167. https://doi.org/10.1016/S0304-3894(97)00039-3.
Lahiri, S. K., and L. Ho. 2011. "Simulation of rapid structural failure due to blast loads from conventional weapons (CONWEP)." In *Proc., NAFEMS World Congress*. Boston: NAFEMS World Congress.
Le Blanc, G., M. Adoum, and V. Lapoujade. 2005. "External blast load on structures–Empirical approach." In *Proc., 5th European LS-DYNA Users Conf.*, 1–12. Solihull, UK: Arup.
Malik, J. 1982. "Yields of the Hiroshima and Nagasaki explosions." In *Reevaluations of dosimetric factors: Hiroshima and Nagasaki*. Los Alamos, New Mexico: Los Alamos National Laboratory.
Markose, A., and C. L. Rao. 2017. "Failure analysis of V-shaped plates under blast loading." *Procedia Eng.* 173: 519–525. https://doi.org/10.1016/j.proeng.2016.12.080.
Masi, F., I. Stefanou, P. Vannucci, and V. Maffi-Berthier. 2019. "Rocking response of inverted pendulum structures under blast loading." *Int. J. Mech. Sci.* 157 (Jul): 833–848. https://doi.org/10.1016/j.ijmecsci.2019.05.024.
Michaloudis, G., and N. Gebbeken. 2019. "Modeling masonry walls under far-field and contact detonations." *Int. J. Impact Eng.* 123 (Jan): 84–97. https://doi.org/10.1016/j.ijimpeng.2018.09.019.
Mougeotte, C., P. Carlucci, S. Recchia, and H. Ji. 2010. *Novel approach to conducting blast load analyses using Abaqus/explicit-CEL*. Picatinny Arsenal, NJ: Army Armament Research Development and Engineering Center.
Netherton, M. D., and M. G. Stewart. 2010. "Blast load variability and accuracy of blast load prediction models." *Int. J. Protect. Struct.* 1 (4): 543–570. https://doi.org/10.1260/2041-4196.1.4.543.
Neuberger, A., S. Peles, and D. Rittel. 2007. "Scaling the response of circular plates subjected to large and close-range spherical explosions. I: Air-blast loading." *Int. J. Impact Eng.* 34 (5): 859–873. https://doi.org/10.1016/j.ijimpeng.2006.04.001.
Newmark, N. M., and J. D. Haltiwanger. 1962. *Air Force design manual: Principles and practices for design of hardened structures*. Technical Documentary Rep. No. AFSC-T1-62-138. Albuquerque, NM: Air Force Special Weapons Center, Kirtland Air Force Base.
PCI (Precast/Prestressed Concrete Institute). 2004 *Design considerations for blast resistance of architectural precast concrete façades*. Designer's Note DN-14. Chicago: PCI.
Perret, W. R. 1956. *Ground-motion studies*. Project 30.2, Operation Redwing, WT-1364. Albuquerque, NM: Sandia.
Perret, W. R. 1960. *Ground motion studies at high incident overpressure*. Project 1.5, Operation Plumbbob, WT-1405. Albuquerque, NM: Sandia.
Perret, W. R., and V. L. Gentry. 1955. *Operation Upshot-Knothole, Project l.4, free-field measurements of earth stress, strain, and ground motion*. Rep. No. WT-716. Albuquerque, NM: Sandia.
Peterson, K. A. 2008. "Numerical simulation investigations in weapon delivery probabilities." Master of Science, Dept. of Mechanical Engineering, Naval Postgraduate School.
Pyle, D. M. 1994. "Stochastic analysis of facilities hardened against conventional weapons effects." Ph.D. thesis, Dept. of Civil Engineering, Univ. of Virginia.
Randers-Pehrson, G., and K. A. Bannister. 1997. *Airblast loading model for DYNA2D and DYNA3D*. Rep. No. ARL-TR-1310. Aberdeen Proving Ground, MD: Army Research Lab.
Rempel, J. R. 1981. *Debris distribution as a parameter in blast/fire interaction*. Menlo Park, CA: SRI International.
Rolph, G. D., F. Ngan, and R. R. Draxler. 2014. "Modeling the fallout from stabilized nuclear clouds using the HYSPLIT atmospheric dispersion model." *J. Environ. Radioact.* 136 (Oct): 41–55. https://doi.org/10.1016/j.jenvrad.2014.05.006.
Salmon, V., and S. R. Hornig. 1953. *Earth acceleration vs time and distance*. SRI Operation Tumbler, WT-517. Stanford, CA: Stanford Research Institute.
Schulte, R. J., and D. W. Dickinson. 1968. *Four methods of solving for the spherical error probable associated with a three-dimensional normal distribution*. Rep. No. MDC-TR-68-12. Alamogordo, NM: Air Force Missile Development Center, Holloman Air Force Base.
Speicher, S. J., and H. L. Brode. 1981. *Airblast overpressure analytical expression for burst heights, range and time over an ideal surface*. PSR Note 385. Santa Monica, CA: Pacific Sierra Research.
Stewart, M. G. 2010. "Risk-informed decision support for assessing the costs and benefits of counter-terrorism protective measures for infrastructure." *Int. J. Crit. Infrastruct. Prot.* 3 (1): 29–40. https://doi.org/10.1016/j.ijcip.2009.09.001.
Stewart, M. G., and M. D. Netherton. 2008. "Security risks and probabilistic risk assessment of glazing subject to explosive blast loading." *Reliab. Eng. Syst. Saf.* 93 (4): 627–638. https://doi.org/10.1016/j.ress.2007.03.007.
Stewart, M. G., M. D. Netherton, and D. V. Rosowsky. 2006. "Terrorism risks and blast damage to built infrastructure." *Nat. Hazards Rev.* 7 (3): 114–122. https://doi.org/10.1061/(ASCE)1527-6988(2006)7:3(114).
Stewart, M. G., M. D. Netherton, Y. Shi, M. Grant, and J. Mueller. 2012. "Probabilistic terrorism risk assessment and risk acceptability for infrastructure protection." *Aust. J. Struct. Eng.* 13 (1): 1–17. https://www.tandfonline.com/doi/abs/10.7158/13287982.2012.11465097.
Swift, L. M., D. C. Sachs, and A. R. Kriebel. 1960. *Air-blast phenomena in the high-pressure region*. Project 1.3, Operation Plumbbob, WT-1403. Menlo Park, CA: Stanford Research Institute.
Swift, L. M., F. M. Sauer, and W. M. Wells. 1958. *Ground motion produced by nuclear detonations*. Project 1.8, Operation Hardtack, WT-1613. Menlo Park, CA: Stanford Research Institute.
Tabatabaei, Z. S., and J. S. Volz. 2012. "A comparison between three different blast methods in LS-DYNA: LBE, MM-ALE, coupling of LBE and MM-ALE." In *Proc., 12th Int. LS-DYNA User Conf.*, 4–5. Detroit: Marriott Detroit Renaissance Center. https://www.dynalook.com/12th-international-ls-dyna-conference/blast-impact20-d.pdf.
Teich, M., and N. Gebbeken. 2010. "The influence of the under pressure phase on the dynamic response of structures subjected to blast loads." *Int. J. Protective Struct.* 1 (2): 219–233. https://doi.org/10.1260/2041-4196.1.2.219.
Toma, J. 1962. *Probability applications to weapon systems analysis*. Rep. No. AFSWC-TDR-62-59, AD-282648. Albuquerque, NM: Air Force Special Weapons Center, Kirtland Air Force Base.
UFC (Unified Facilities Criteria). 2008. *Structures to resist the effects of accidental explosions*. Rep. No. UFC 3-340-02. Washington, DC: US Army Corps of Engineers, Naval Facilities Engineering Command, Air Force Civil Engineer Support Agency.
US Army. 1986. *Fundamentals of protective design for conventional weapons*. Technical Manual TM 5-855-1. Washington, DC: Dept. of Army.
Van Der Voort, M. M., and J. Weerheijm. 2013. "A statistical description of explosion produced debris dispersion." *Int. J. Impact Eng.* 59 (Sep): 29–37. https://doi.org/10.1016/j.ijimpeng.2013.03.002.
Willis, H. H., A. R. Morral, T. K. Kelly, and J. J. Medby. 2006. *Estimating terrorism risk*. RAND/MG-388-RC. Santa Monica, CA: Rand.